Available online at www.sciencedirect.com
SCIENCE DIRECT®
Geochimica et Cosmochimica Acta 70 (2006) 1977–1994
Geochimica
www.elsevier.com/locate/gca

Secular variation in the major-ion chemistry of seawater: Evidence from fluid inclusions in Cretaceous halites

Michael N. Timofeeff [a,*], Tim K. Lowenstein [a], Maria Augusta Martins da Silva [b], Nicholas B. Harris [c]

[a] Department of Geological Sciences and Environmental Studies, State University of New York at Binghamton, Binghamton, NY 13902, USA
[b] Departamento de Geologia, Universidade Federal Fluminense, Niteroi, Rio de Janeiro, Brazil
[c] Department of Geology and Geological Engineering, Colorado School of Mines, Golden, CO 80401, USA

Received 22 August 2005; accepted in revised form 17 January 2006

Abstract

The major-ion (Mg^{2+}, Ca^{2+}, Na^{+}, K^{+}, SO_4^{2-}, and Cl^{-}) chemistry of Cretaceous seawater was determined from analyses of seawater-derived brines preserved as fluid inclusions in marine halites. Fluid inclusions in primary halite from three evaporite deposits were analyzed by the environmental scanning electron microscopy (ESEM) X-ray energy dispersive spectrometry (EDS) technique: the Early Cretaceous (Aptian, 121.0–112.2 Ma) of the Sergipe basin, Brazil and the Congo basin, Republic of the Congo, and the Early to Late Cretaceous (Albian to Cenomanian, 112.2–93.5 Ma) of the Khorat Plateau, Laos, and Thailand. The fluid inclusions in halite indicate that Cretaceous seawater was enriched several fold in Ca^{2+}, depleted in SO_4^{2-}, Na^{+}, and Mg^{2+}, and had lower Na^{+}/Cl^{-}, Mg^{2+}/Ca^{2+}, and Mg^{2+}/K^{+} ratios compared to modern seawater. Elevated Ca^{2+} concentrations, with $Ca^{2+} > SO_4^{2-}$ at the point of gypsum saturation, allowed Cretaceous seawater to evolve into Mg^{2+}–Ca^{2+}–Na^{+}–K^{+}–Cl^{-} brines lacking measurable SO_4^{2-}.The major-ion composition of Cretaceous seawater was modeled from fluid inclusion chemistries for the Aptian and the Albian-Cenomanian. Aptian seawater was extreme in its Ca^{2+} enrichment, more than three times higher than present day seawater, with a Mg^{2+}/Ca^{2+} ratio of 1.1–1.3. Younger, Albian-Cenomanian seawater had lower Ca^{2+} concentrations, and a higher Mg^{2+}/Ca^{2+} ratio of 1.2–1.7. Cretaceous (Aptian) seawater has the lowest Mg^{2+}/Ca^{2+} ratios so far documented in Phanerozoic seawater from fluid inclusions in halite, and within the range chemically favorable for precipitation of low-Mg calcite ooids and cements. Results from halite fluid inclusions, together with Mg^{2+}/Ca^{2+} ratios measured from echinoderm and rudist calcite, all indicate that Early Cretaceous seawater (Hauterivian, Barremian, Aptian, and Albian) had lower Mg^{2+}/Ca^{2+} ratios than Late Cretaceous seawater (Coniacian, Santonian, and Campanian). Low Aptian-Albian Mg^{2+}/Ca^{2+} seawater ratios coincide with negative excursions of $^{87}Sr/^{86}Sr$ ratios and $\delta^{34}S_{SO_4}$, and peak Cretaceous ocean crust production rates, all of which suggests a link between seawater chemistry and midocean ridge hydrothermal brine flux.

1. Introduction

The Phanerozoic oceans have undergone two oscillations in major-ion chemistry (Mg^{2+}, Ca^{2+}, Na^{+}, K^{+}, SO_4^{2-}, and Cl^{-}) (Kovalevich et al., 1998; Lowenstein et al., 2001, 2003; Dickson, 2002; Horita et al., 2002; Steuber and Veizer, 2002) that generally match the timing of 100–200 million-year oscillations in sea level, icehouse–greenhouse climates, and global volcanicity (Fischer, 1980; Hardie, 1996). Such cyclic variations in seawater chemistry are now accepted by the geological community but their causes are debated.

This paper reports the major-ion chemical composition of Cretaceous seawater from fluid inclusions in marine halites. The Cretaceous was a time of hothouse climate, elevated atmospheric CO_2, relatively warm surface and deep ocean waters, and high sea levels. Polar climates with mean annual air temperatures above 14 °C are inferred from Late Cretaceous vertebrates from the Canadian Arctic (Tarduno

* Corresponding author. Fax: +1 607 777 2288.
E-mail addresses: mtimofee@binghamton.edu (M.N. Timofeeff), Lowenst@binghamton.edu (T.K. Lowenstein), augusta@igeo.uff.br (M.A.M. da Silva), nbharris@mines.edu (N.B. Harris).

0016-7037/$ - see front matter © 2006 Elsevier Inc. All rights reserved.
doi:10.1016/j.gca.2006.01.020

et al., 1998), and correspondingly warm polar oceans are suggested by Mid to Late Cretaceous Arctic Ocean sea surface temperatures of 15–20 °C (Jenkyns et al., 2004). Similar extreme warmth, such as the 18 °C deep waters and >30 °C surface waters at 59° S paleolatitude during the Late Cretaceous (Turonian), is also documented in the southern hemisphere (Huber, 1998). Land-sea configuration and enhanced poleward oceanic heat transport contributed to the Cretaceous warmth. However, mantle superplumes, elevated ocean crust production, and associated mantle outgassing at 50–100% above modern rates between 80 and 125 Ma offer the best explanation for the extreme Cretaceous climates, sea levels and atmospheric CO_2 (Larson, 1991).

One predicted consequence of high rates of ocean crust production in the Cretaceous is enhanced midocean ridge (MOR) hydrothermal brine circulation, which, in turn, would have led to significant changes in the major-ion chemistry of seawater (Hardie, 1996; Demicco et al., 2005). Seawater compositional changes would have resulted from increases in the flux of components derived from the midocean ridges relative to the riverine flux of major-ion components. Significant changes in the major-ion chemistry of Cretaceous seawater may have influenced the mineralogy of abiotically precipitated marine carbonates and biocalcifying organisms (Sandberg, 1983; Wilkinson et al., 1985; Stanley and Hardie, 1998; Stanley et al., 2002; Ries, 2004). Variations in seawater composition may also explain the "anomalous" Cretaceous evaporites from Brazil, Congo, and Thailand that contain the extremely rare $CaCl_2$-bearing mineral tachyhydrite (see Table 1 for mineral formulas) and completely lack the $MgSO_4$ salts formed from evaporation of modern seawater (Wardlaw, 1972a; Hite and Japakesetr, 1979).

The purpose of this study is to determine the major-ion composition of Cretaceous seawater from chemical analyses of fluid inclusions in primary marine halites. Fluid inclusions in halite from three evaporite deposits were studied: the Early Cretaceous (Aptian, 121.0–112.2 Ma) of the Sergipe basin, Brazil and Congo basin, and the Early to Late Cretaceous (Albian to Cenomanian, 112.2–93.5 Ma) of the Khorat Plateau, Laos, and Thailand. First, we review the geologic background of the halites and fluid inclusions under investigation and examine their possible seawater origin. Second, we employ the chemical composition of the fluid inclusions to show that Cretaceous seawater was enriched in Ca^{2+}, depleted in Na^{+}, Mg^{2+}, and SO_4^{2-}, and had a low Mg^{2+}/Ca^{2+} compared to modern seawater. Third we model the major-ion composition of Cretaceous seawater for two intervals (Aptian and Albian-Cenomanian) applying the Harvie–Møller–Weare (HMW) computer program (Harvie et al., 1984) to the fluid inclusion chemistries. Finally, we compare the fluid inclusion record of Cretaceous seawater with other Cretaceous paleoceanographic data. The results presented here in detail were published in preliminary form as Cretaceous seawater Mg^{2+}/Ca^{2+} ratios (Lowenstein et al., 2001, Fig. 2) and as concentrations of Ca^{2+} and SO_4^{2-} (Lowenstein et al., 2003, Fig. 1 and Table DR1).

Table 1
Minerals discussed in this paper and their formulas

Mineral	Formula
Calcite	$CaCO_3$
Aragonite	$CaCO_3$
Dolomite	$CaMg(CO_3)_2$
Magnesite	$MgCO_3$
Gypsum	$CaSO_42H_2O$
Anhydrite	$CaSO_4$
Halite	NaCl
Polyhalite	$K_2Ca_2Mg(SO_4)_42H_2O$
Kieserite	$MgSO_4H_2O$
Sylvite	KCl
Carnallite	$KMgCl_36H_2O$
Tachyhydrite	$CaMgCl_412H_2O$
Bischofite	$MgCl_26H_2O$

2. Sampling and analysis

2.1. Sample descriptions: Geologic background and previous work

2.1.1. Sergipe and congo salt basins

The Sergipe and Congo salts formed during the early rifting phase of formation of the South Atlantic Ocean (Fig. 1) (Evans, 1978; Burke and Sengor, 1988; Coward et al., 1999). Both deposits are approximately the same age (Aptian, 121.0–112.2 Ma), contain the same evaporite minerals, including the rare $CaCl_2$-bearing mineral tachyhydrite, and occur stratigraphically above marine and nonmarine siliciclastic sediments and below fully marine limestones (Wardlaw and Nicholls, 1972; Evans, 1978). They have been interpreted as marine transgressive sediments of the proto Atlantic Ocean deposited in a tectonic setting similar to the modern Red Sea (Wardlaw, 1972a; Wardlaw and Nicholls, 1972; Evans, 1978; Silva, 1983).

The Sergipe basin occurs on the northeastern continental margin of Brazil, and extends offshore, with a total aerial extent of ~20,000 km^2 (Fig. 1A) (Silva, 1983). Jurassic and Early Cretaceous fluvial-lacustrine siliciclastics and carbonates are overlain by the Aptian Muribeca Formation (Wardlaw, 1972a; Silva, 1983; Coward et al., 1999). The Ibura Member of the Muribeca Formation is an evaporite sequence up to 800 m thick (Fig. 2A) (Oliver, 1997). Planktonic and benthic foraminifera and ammonoids in the overlying Riachuelo Formation carbonates indicate open marine conditions (Schaller, 1969).

The vertical evaporite mineral succession in the Ibura Member is, in general, anhydrite, halite, carnallite, sylvite, and tachyhydrite, with beds of tachyhydrite as thick as 100 m (Table 1, Fig. 2A). Preservation of primary sedimentary features in some Ibura Member evaporites suggests little post-depositional alteration and mineralogical changes. Primary features identified include laminated halite, fluid inclusion-banded chevron halite, and vertically oriented

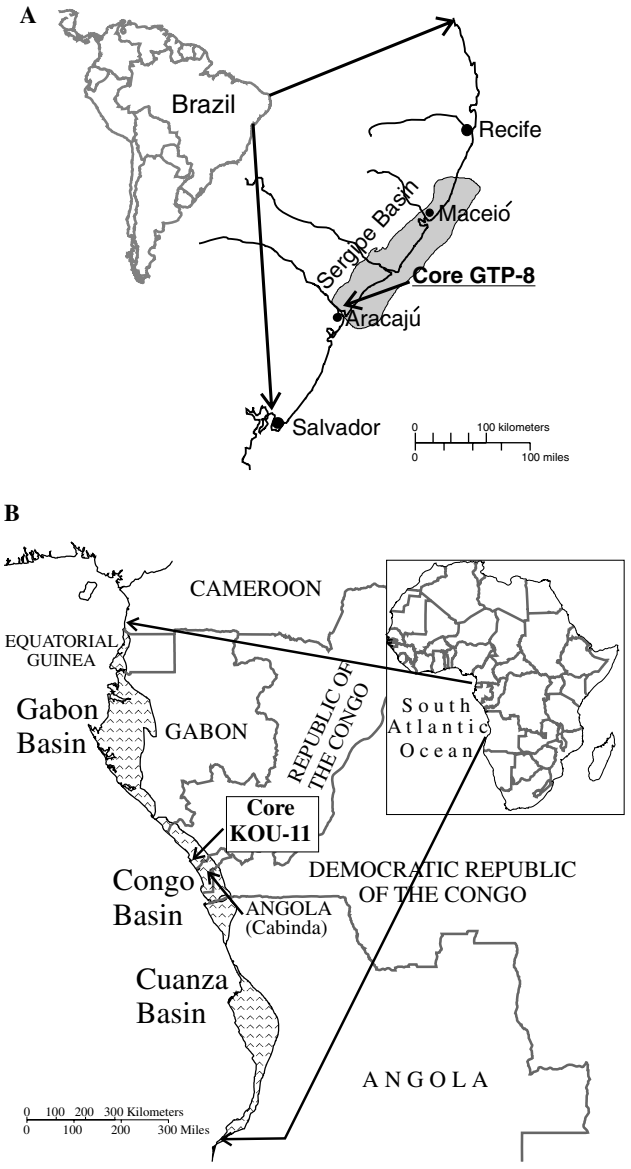

Fig. 1. (A) Location of the Sergipe basin, continental margin, northeastern Brazil, (modified from Silva, 1983). Core GTP-8 was sampled from the Ibura Member of the Muribeca Formation. (B) The Congo basin is one of several Lower Cretaceous basins along western Africa, which include from north to south the Douala basin (Cameroon), the Gabon basin, the Congo basin (Republic of the Congo, Democratic Republic of the Congo, Angola), and the Cuanza (Kwanza) basin (Angola) (modified from de Ruiter, 1979). Location of core KOU-11, Loeme Formation, Pointe-Noire, Congo basin, Republic of the Congo, is shown with arrow.

carnallite crystals draped by halite laminites (Wardlaw, 1972b; Szatmari et al., 1979; Oliver, 1997). Diagenetically formed displacive halite occurs in some layers (Oliver, 1997). The lowermost part of the Ibura Member from core GTP-8 core was studied by Oliver (1997). Fluid inclusions from two primary chevron halite layers, from the base of the Ibura Member in core GTP-8, at depths of 768 m and 792 m, were analyzed in this study (Fig. 2A).

All workers have noted the primary nature of the evaporites from Sergipe, and there is general agreement that the chloride salts are unaltered subaqueous deposits. The unusual evaporite mineralogy, however, has been the source of much discussion. It has long been recognized that the Ibura Member evaporites are depleted in $CaSO_4$ and lack the $MgSO_4$ salts (for example, polyhalite and kieserite) that form during the evaporation of modern seawater. The $CaCl_2$-bearing salt tachyhydrite indicates that the parent waters were enriched in $CaCl_2$ with equivalents $Ca^{2+} > SO_4^{2-} + HCO_3^-$ because after evaporation and precipitation of calcium carbonate and gypsum, calcium but not sulfate remained in the later brines. These Early Cretaceous waters therefore had a chemical composition different from modern seawater (Wardlaw, 1972a). Br^- measurements from halites of the Ibura Member have values up to 200 parts per million (ppm) in the halite–anhydrite facies (Szatmari et al., 1974). These values of Br^- in halite are similar to those in other marine evaporites (Holser, 1979), which suggests the Ibura Member salts formed from Cretaceous seawater.

The Congo basin is one of several Lower Cretaceous basins developed along the western continental margin of Africa, including the Gabon, the Congo, and the Cuanza (or Kwanza) basins (Fig. 1B) (de Ruiter, 1979; Nürnberg and Müller, 1991; Maurin and Guiraud, 1993). The Mesozoic basins of west Africa contain clastic and carbonate "rift sediments" of Late Jurassic to middle Aptian age, locally underlain by Permian to Middle Jurassic nonmarine siliciclastics (Coward et al., 1999). In the Congo basin, these are the Vandji, Sialivakou, Djeno, Marnes Noires, and Argilles Vertes Formations (Harris, 2000). Unconformably overlying the rift sequence is a relatively thin clastic and carbonate sequence known as the Gamba Formation in Gabon and Chela Formation in Congo, which contain marine foraminifera, ammonites, and pelecypods (Evans, 1978). These formations are interpreted to record marine flooding (Evans, 1978). The Late Aptian salts (Loeme Formation) examined in this study conformably overlie the Chela Formation, which, in turn, are overlain by Albian to Cenomanian marine carbonates, the Couches de la Mavuma and Pinda Formations of the Congo basin (Evans, 1978; de Ruiter, 1979; Coward et al., 1999).

The Aptian evaporites from the Congo basin examined in this study come from the Loeme Formation, core KOU-11, Pointe Noire, Republic of the Congo (Fig. 2B). In this core, the Loeme evaporites are ~700 m thick with a general mineral sequence of halite, carnallite, and bischofite + tachyhydrite (Wardlaw and Nicholls, 1972; de Ruiter, 1979). Twenty-three thin sections were prepared from core KOU-11 samples of halite and anhydrite from depths of 573–870 m. Primary textures and fabrics were observed in most samples including chevron halite, halite laminites to thin beds with cumulate crystal cubes, rafts, and skeletal crystals. Fluid inclusions analyzed came from chevron halite in the upper part of the Loeme Formation, at depths of 746, 780, and 869 m.

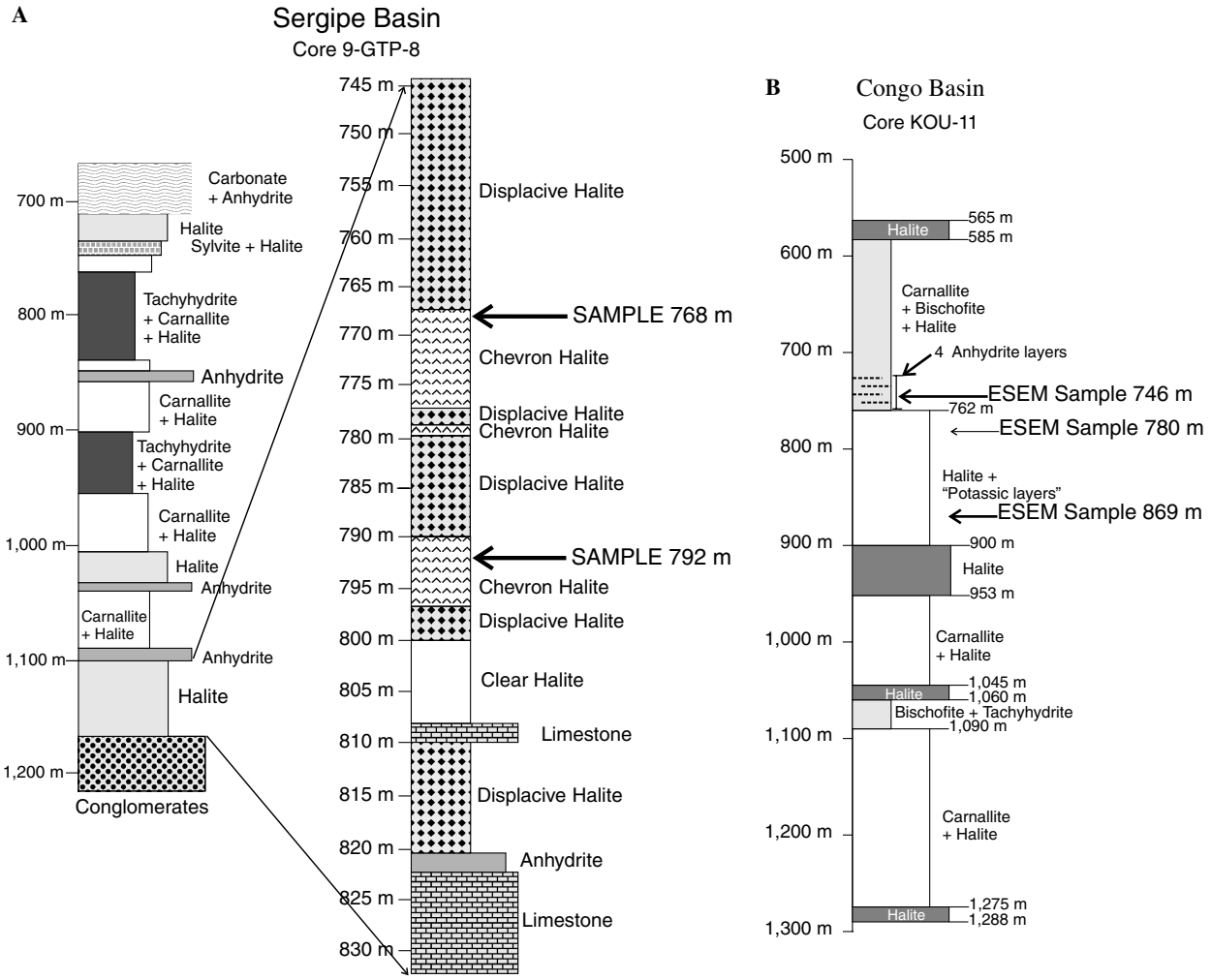

Fig. 2. (A) Complete stratigraphic section of the Ibura Member of the Muribeca Formation on left (modified from Fig. 4 of Wardlaw, 1972a). The lowermost part of the Ibura Member, core GTP-8, is shown on the right (modified from Oliver, 1997). The first cycle of the Ibura Member (833–766 m) contains laminated limestone, nodular anhydrite, displacive halite, bituminous shale, stromatolitic limestone, and halite (laminated, chevron, and displacive) (Oliver, 1997). Fluid inclusions from two chevron halite layers (792 and 768 m) were analyzed in this study. (B) Stratigraphic section of the Loeme Formation, core KOU-11, Republic of the Congo. Fluid inclusions were analyzed from chevron halites at depths of 869, 780, and 746 m.

2.1.2. Khorat Plateau, Laos, and Thailand

The Maha Sarakham Formation evaporites occur on the Khorat Plateau of Thailand and Laos (Fig. 3A) (Hite and Japakesetr, 1979). The plateau is divided by the Phu Phan anticlinorium into the Sakon Nakhon basin to the north and the Khorat basin to the south (Hite and Japakesetr, 1979; El Tabakh et al., 1999). The bedrock of the Khorat Plateau, the Khorat Group, consists of up to 5 km of Late Triassic to late Early Cretaceous fluvial and lacustrine red beds. The overlying Maha Sarakham Formation has been dated using palynomorphs (Sattayarak et al., 1991; Smith et al., 1996) as Albian to Cenomanian in age (112.2–93.5 Ma). Tertiary nonmarine mudstones of the Phu Tok Formation overlie the Maha Sarakham Formation.

The Maha Sarakham Formation is divided into three depositional cycles (Lower, Middle, and Upper Members) each of which contains an evaporite sequence capped by nonmarine siliciclastic redbeds (Fig. 3B) (Hite and Japakesetr, 1979; Utha-Aroon, 1993; El Tabakh et al., 1999). The Lower Member contains the basal anhydrite overlain by halite, with primary evaporites including chevron halite and laminated anhydrite (Utha-Aroon, 1993; El Tabakh et al., 1999). The halite unit is capped with potash salts (carnallite, sylvite, and tachyhydrite) and borate minerals (Hite and Japakesetr, 1979). Siliciclastic redbeds, composed of disrupted "chaotic" mudstones, occur above the potash evaporites (Utha-Aroon, 1993; El Tabakh et al., 1999). Two more evaporite-siliciclastic redbed cycles occur as the Middle and Upper Members of the Maha Sarakham Formation (Fig. 3B) (El Tabakh et al., 1999).

The L-1 core was drilled through the Maha Sarakham Formation in the Sakon Nakhon basin, near Vientienne, Laos (Fig. 3A) (Hite, 1974; Hite and Japakesetr, 1979). In this well, the basal anhydrite is overlain by ~300 m of halite (Fig. 3B) (Hite, 1974). The Potash Unit in core L-1 is composed of sylvite and halite, which, in turn, is overlain by mudstone redbeds (Hite, 1974). Fluid inclusions in

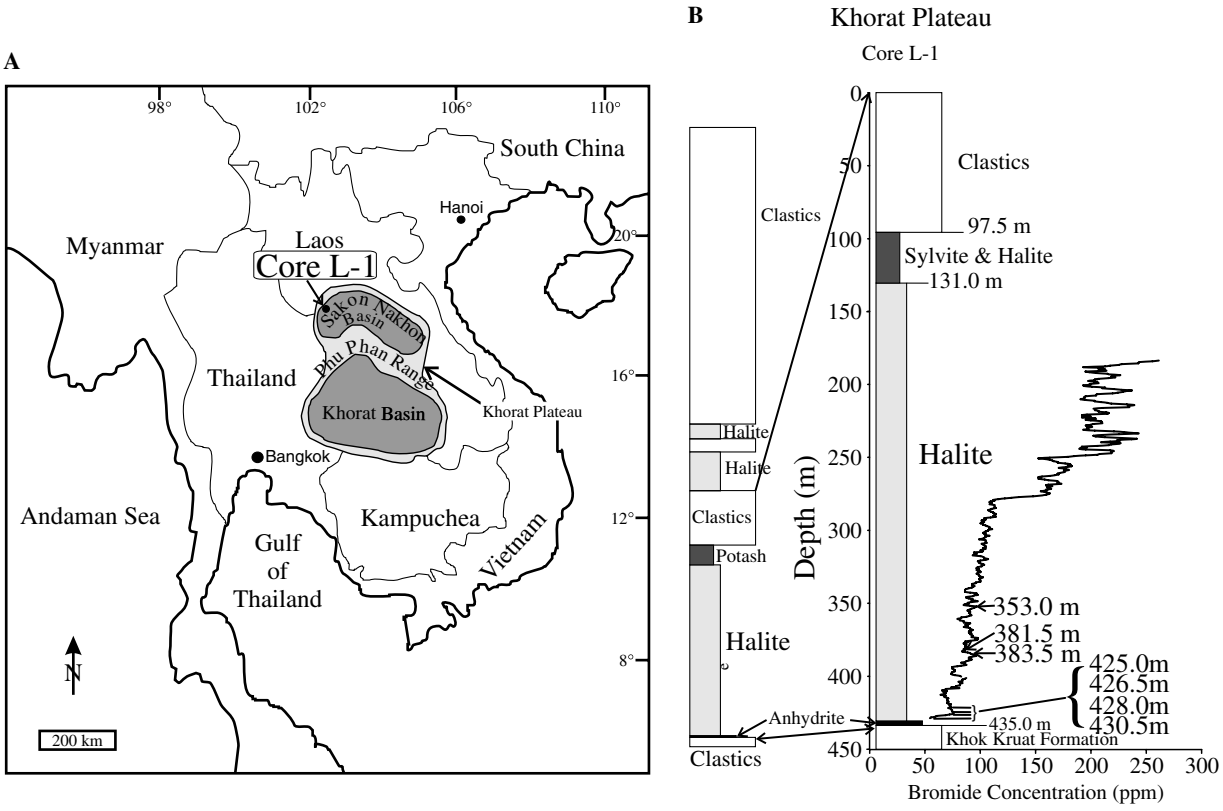

Fig. 3. (A) The Maha Sarakham Formation salts occur over an area of 60,000 km^2 on the Khorat Plateau, northeastern Thailand, and central Laos. Core L-1 was drilled through the Maha Sarakham Formation near Vientienne, Laos (modified from Hite, 1974; Hite and Japakesetr, 1979; El Tabakh et al., 1999). (B) The complete Maha Sarakham Formation (left) is composed of three depositional cycles (Lower, Middle, and Upper Members) each with an evaporite sequence overlain by siliciclastic redbeds (modified from El Tabakh et al., 1999). Core L-1 (right) through the Lower Member contains anhydrite overlain by ~300 m of halite, with primary cumulates and chevrons (Hite, 1974; Hite and Japakesetr, 1979). The Potash Unit in core L-1 is composed of sylvite and halite, and is overlain by mudstone redbeds. Fluid inclusions in halite of the Lower Member were analyzed from 430.5, 428.0, 426.5, 425.0, 383.5, 381.5, and 353 m. Br^- concentrations in halite (right) from the L-1 core show a progressive increase up section from 60 to 250 ppm (modified from Hite and Japakesetr, 1979).

halite of the Lower Member of the Maha Sarakham Formation were analyzed from seven stratigraphic intervals at 430.5, 428.0, 426.5, 425.0, 383.5, 381.5, and 353.0 m.

The marine versus nonmarine origin of the Maha Sarakham evaporites is debated. Like the Aptian evaporites from the Sergipe and Congo basins, the mineral sequence of halite–carnallite–sylvite–tachyhydrite cannot form by evaporation of modern seawater. Hite and Japakesetr (1979, p. 457) suggested that the parent water of the Maha Sarakham evaporites was seawater, but "the chemistry of the Cretaceous ocean was somehow different from that of the modern ocean". Utha-Aroon (1993) argued for a nonmarine origin on the basis of the features in the associated clastic redbed units (desiccation cracks, caliche, and anhydrite nodules). The redbeds in the Maha Sarakham Formation, and the underlying continental sediments of the Khorat Group, suggest a nonmarine setting for the siliciclastic sediments associated with the Maha Sarakham evaporites. However, other features suggest flooding of the Khorat Plateau by seawater, precipitation of evaporites, and drying up of the basin three times, leading to the formation of the three observed evaporite-redbed sequences. Hite and Japakesetr (1979) and El Tabakh et al. (1999) noted that the number and thickness of anhydrite layers increases on the western side of the Sakon Nakhon and Khorat basins, which suggests a western connection with the Cretaceous Tethys Sea. Sulfur isotopes in the anhydrites of the Maha Sarakham evaporites have Cretaceous seawater values ($\delta^{34}S$ 14.3–17.7‰) whereas sulfur isotopes in the anhydrites of the redbeds do not have Cretaceous seawater values ($\delta^{34}S$ 6.4–10.9‰) (El Tabakh et al., 1999). Br^- concentrations in halites from many cores through the Lower Member of the Maha Sarakham Formation generally are 40–60 ppm at the base, with a gradual increase up the stratigraphic section to values of 200–300 ppm in the uppermost halites (Hite and Japakesetr, 1979; El Tabakh et al., 1999). The Br^- profile from the L-1 core, with values increasing up section from 60 to 250 ppm, is shown in Fig. 3B (Hite and Japakesetr, 1979). This Br^- profile, with steadily increasing values, and with highest values closest to the overlying potash interval, suggests progressive evaporation of a large body of brine. The range of Br^- in halite from the Lower Member of the Maha Sarakham Formation (60–250 ppm) is similar to that in other marine evaporites (Holser, 1979), which suggests a Cretaceous seawater

parentage. In summary, the interpretation of the Maha Sarakham Formation most compatible with geologic and geochemical data is that the Khorat plateau region was flooded three times by the Cretaceous ocean. Siliciclastic redbeds capping each evaporite interval represent continental conditions between marine flooding events.

2.2. Criteria for sample selection

Primary halites crystallized from evaporating surface brines are used for fluid inclusion analysis. Halites precipitated from surface brines occur in layers of cumulate crystals (sunken cubes, skeletal hoppers, and rafts formed at the air-brine interface) and as bottom-grown crusts (fluid inclusion-banded chevrons) (Lowenstein and Hardie, 1985). These types of primary, subaqueous-grown halite can be distinguished petrographically from diagenetic halite cement and recrystallized halite (Hardie et al., 1985). Chevron halite, with alternating bands rich (cloudy) and poor (clear) in fluid inclusions, is well suited for fluid inclusion analysis because it commonly contains primary inclusions >30 μm in size.

Fluid inclusions in halite that formed in large perennial brine bodies are ideal for determining the chemistry of the parent waters. The great mass of dissolved salt in large brine bodies make modification of the major-ion chemistry by syndepositional recycling processes or nonmarine inflow waters less likely than in shallow/ephemeral systems. Syndepositional recycling occurs, for example, when seawater inundates an evaporite basin and dissolves preexisting salts. This recycling increases the proportion of those ions derived from the dissolved minerals (e.g., Na^+ and Cl^- from halite, K^+, Mg^{2+}, and Cl^- from carnallite) in the now chemically modified seawater. Evaporative concentration of such altered seawater will produce brines with a different chemical composition from brines evolved from pristine seawater. Clearly, halite deposits that formed in paleoenvironments in which significant recycling occurred cannot be used for study of ancient seawater chemistry.

In this study, halite samples were analyzed that contained primary subaqueous textures and no petrographic evidence for syndepositional dissolution. Petrographic criteria, however, cannot rule out the possibility that the chemical composition of the parent seawater has not been modified either by recycling of previously deposited salts in a more marginal location or by nonmarine inflow waters. Therefore, a nonpetrographic criterion for seawater parentage was applied to all analyzed fluid inclusions. This criterion requires that the major ion chemistry of an individual fluid inclusion must lie on the evaporation curve defined by the entire suite of fluid inclusions from the same deposit. Individual fluid inclusions whose chemical compositions do not fall on the defined evaporation curve must have formed from chemically-modified parent seawaters, and were therefore excluded from calculations of seawater chemistry.

Halites formed near the bottom of the evaporite section commonly show little evidence of recycling and such samples were preferred. These include the basal halite of the Ibura Member of the Muribeca Formation, Brazil, and the Lower Halite Member of the Maha Sarakham Formation, Laos. No samples were available from the lowermost halites of the Congo basin. Fluid inclusions analyzed from the Congo basin come from halites that lie above potash salts (Fig. 2B). The chemistry of the parent waters of the Congo basin halites may have been influenced to some extent by recycling of the underlying potash salts.

2.3. Analytical techniques

Fluid inclusions were analyzed using an environmental scanning electron microscope (ESEM) with X-ray energy dispersive analysis (EDS) capabilities (Timofeeff et al., 2000). The ESEM X-ray EDS technique measures absolute ionic concentrations (Ca, Mg, K, S in sulfate, and Cl) in frozen inclusions at concentrations above ~0.1 wt.%. For Na, quantitative analyses were achieved at concentrations above 0.5 wt.%. This technique is capable of producing accurate major element chemical analyses of individual frozen fluid inclusions in halite greater than ~30μm in size (Timofeeff et al., 2000). Accuracies for the major elements in aqueous standards were better than 7% and precisions (relative standard deviations) ranged from 2% to 7%. Results on fluid inclusions in laboratory-grown halite gave accuracies of 6–10% for Mg, Ca, and K and precisions from 3% to 16%. The chemical analyses reported here were done on frozen fluid inclusions with flat surfaces and homogeneous glass-like textures. Chemical analyses reported in Tables 2a–c represent the average chemical composition of between 3 and 5 analyses taken from one fluid inclusion with relative standard deviations less than 10%.

2.4. Computer modeling

Computer models are needed for the quantitative treatment of evaporation of natural waters and the accompanying mineral precipitation and dissolution. We used the ion interaction model and parameters of Harvie et al. (1984) (HMW) for several aspects of this study. First, the HMW computer program was used to simulate equilibrium evaporation of modern seawater at 25°C; concentrations, in molalities, of all the major ions at each evaporation step were calculated along with the number of moles of salts precipitated during each evaporation step. Such simulated evaporation paths have been shown to closely match the chemical compositions of natural brines, fluid inclusion waters, and the mineralogical sequences in bedded evaporites (Harvie et al., 1980, 1984; Casas et al., 1992; Timofeeff et al., 2001).

The HMW computer program was also used to simulate the evaporation of Cretaceous seawater, on the basis of the chemical composition of the brine inclusions from the Sergipe, Congo, and Khorat Plateau halites. Finally, the HMW

Table 2a
The major-ion chemical composition of individual primary fluid inclusions in halite from the Aptian (121.0–112.2 Ma) Muribeca Formation, Sergipe basin, Brazil, borehole core GTP-8

Mg	K	Ca	Na	Cl	Sample
540	180	420	4300	6410	GTP-8 A-56 792.2 m
970	250	570	3300	6630	GTP-8 A-56 792.2 m
1090	260	570	3130	6730	GTP-8 A-56 792.2 m
1100	240	630	3040	6750	GTP-8 A-56 792.2 m
710	220	560	3780	6540	GTP-8 A-56 792.2 m
910	240	620	3340	6660	GTP-8 A-56 792.2 m
1010	240	640	3170	6710	GTP-8 A-56 792.2 m
1130	250	640	2980	6780	GTP-8 A-56 792.2 m
360	190	500	4480	6400	GTP-8 A-56 792.2 m
900	250	600	3400	6650	GTP-8 A-56 792.2 m
860	230	600	3460	6620	GTP-8 A-56 792.2 m
1120	290	640	2990	6800	GTP-8 A-56 792.2 m
1460	310	680	2430	7030	GTP-8 A-56 792.2 m
1630	180	940	1950	7260	GTP-8 A-56 792.2 m
2590	250	2240	320	10210	GTP-8 SE A-100 768.2 m
1830	210	1820	900	8410	GTP-8 SE A-100 768.2 m
2790	190	2190	270	10420	GTP-8 SE A-100 768.2 m
1560	170	1580	1330	7790	GTP-8 SE A-100 768.2 m
2420	190	2230	370	9880	GTP-8 SE A-100 768.2 m
1190	150	1780	1530	7620	GTP-8 SE A-100 768.2 m
1930	200	2040	700	8820	GTP-8 SE A-100 768.2 m

All values are millimolal (mmol per kg H_2O). Na^+ and Cl^- concentrations were normalized to halite saturation at 25 °C using the HMW computer program. Fluid inclusions with gray shading generally contain concentrated brines more likely to have undergone syndepositional chemical modifications (see text). Such inclusions were eliminated from calculations of Cretaceous seawater composition.

Table 2b
The major-ion chemical composition of individual primary fluid inclusions in halite from the Aptian (121.0–112.2 Ma) Loeme Formation, Congo basin, Congo from borehole core KOU-11

Mg	K	Ca	Na	Cl	Sample
1580	220	1060	1830	7330	A746Con1 May04A 746 m
1020	200	930	2760	6850	A746Con2 May04A 746 m
910	180	870	3000	6750	B746Con1 May04B 746 m
800	170	830	3240	6680	B746Con2 May04B 746 m
2140	160	1320	1020	8100	AConB3 Apr28A 780 m
1180	150	1310	2060	7200	BConB1 Apr28B 780 m
1980	160	1600	950	8270	BConB2 Apr28B 780 m
2520	140	2610	240	10640	ACon1 Feb16A 869 m
3010	130	2780	130	11840	ACon2 Feb16A 869 m
2750	150	2700	180	11240	ACon3 Feb16A 869 m
2770	140	2640	190	11140	ACon4 Feb16A 869 m
2120	110	2250	500	9340	BCon1 Feb13B 869 m
1220	90	1970	1330	7800	BCon2 Feb13B 869 m
2840	130	2590	180	11170	ACon1 Feb13A 869 m
2170	100	2350	430	9580	ACon2 Feb13A 869 m
2640	120	2460	250	10570	ACon3 Feb13A 869 m

All values are millimolal (mmol per kg H_2O). Na^+ and Cl^- concentrations were normalized to halite saturation at 25 °C using the HMW computer program. Fluid inclusions with gray shading generally contain concentrated brines more likely to have undergone syndepositional chemical modifications (see text). Such inclusions were eliminated from calculations of Cretaceous seawater composition.

computer program was used to calculate the concentrations of Na^+ and Cl^- in fluid inclusions. Fluid inclusions less than ~150 μm in size analyzed by the ESEM X-ray

Table 2c
The major-ion chemical composition of individual primary fluid inclusions in halite from the Albian-Cenomanian (112.2–93.5 Ma) Maha Sarakham Formation, Sakon Nakhon basin, Laos, from borehole core L-1

Mg	K	Ca	Na	Cl	Sample
930	350	340	3710	6590	353 m
860	390	290	3890	6570	353 m
780	400	370	3890	6590	353 m
1180	420	390	3210	6760	353 m
620	320	320	4270	6480	353 m
690	310	330	4210	6550	353 m
740	360	350	4000	6550	353 m
800	380	340	3920	6570	353 m
640	330	300	4270	6480	353 m
740	320	310	4080	6510	353 m
850	250	270	3990	6480	381 m
570	250	290	4450	6410	381 m
850	260	280	3980	6490	381 m
610	210	280	4420	6400	381 m
550	190	290	4510	6370	381 m
620	270	330	4280	6450	383.5 m
780	260	240	4160	6450	383.5 m
570	230	280	4470	6400	383.5 m
1190	230	250	3430	6540	425 m
1150	220	280	3460	6550	425 m
720	240	280	4200	6450	426.5 m
680	290	300	4220	6460	426.5 m
710	240	250	4250	6410	428 m
880	200	250	4000	6460	428 m
700	200	220	4340	6390	428 m
740	190	240	4270	6410	428 m
470	240	240	4710	6360	430.5 m
1070	220	300	3570	6530	430.5 m
1040	230	360	3540	6570	430.5 m
800	200	360	3960	6480	430.5 m
1110	250	360	3420	6620	430.5 m
560	230	290	4480	6400	430.5 m
580	220	240	4510	6380	430.5 m
560	230	220	4590	6370	430.5 m
620	210	280	4380	6390	430.5 m
1060	220	260	3660	6520	430.5 m
690	270	240	4320	6440	430.5 m
820	210	290	4030	6460	430.5 m
830	240	270	4030	6470	430.5 m
1470	470	350	2790	6900	353 m
1330	190	490	2890	6710	425 m
1590	170	330	2750	6760	425 m
1440	140	320	2930	6590	425 m
1190	160	750	2760	6800	428 m
1120	170	800	2800	6800	428 m
1880	170	590	2040	7160	428 m
900	140	680	3330	6640	428 m
690	210	300	4780	6950	430.5 m
2200	100	510	1730	7230	430.5 m
1350	140	400	3000	6640	430.5 m
2270	90	400	1760	7180	430.5 m
2420	80	510	1440	7360	430.5 m
2350	140	480	1600	7410	430.5 m
1240	250	310	3270	6610	430.5 m
1040	140	360	3560	6500	430.5 m
1330	200	330	3100	6630	430.5 m
1200	130	480	3130	6610	430.5 m
1100	210	280	3450	6420	430.5 m

All values are millimolal (mmol per kg H_2O). Na^+ and Cl^- concentrations were normalized to halite saturation at 25 °C using the HMW computer program. Fluid inclusions with gray shading generally contain concentrated brines more likely to have undergone syndepositional chemical modifications (see text). Such inclusions were eliminated from calculations of Cretaceous seawater composition.

EDS technique produce spectra for Na^+ and Cl^- that are anomalously large because scattered electrons from the primary beam excite the host halite crystal. In these cases, Na^+ and Cl^- concentrations cannot be determined from ESEM X-ray EDS data but must be computed for halite-saturated conditions using the HMW computer program at specified molalities of Mg^{2+}, Ca^{2+}, and K^+ (Timofeeff et al., 2000).

3. Results

3.1. Major-ion chemistry of Cretaceous fluid inclusions

Concentrations of Na^+, Mg^{2+}, Ca^{2+}, K^+, and Cl^- in fluid inclusions, in millimolalities (mmolal, mmol per kg H_2O), from the Sergipe basin (21 fluid inclusions), the Congo basin (16 fluid inclusions), and the Khorat Plateau (58 fluid inclusions) are shown in Tables 2a–c and in plots versus Cl^- (Figs. 4A–D and 5A–D), Ca^{2+} (Figs. 4E,F and 5E,F), and Mg^{2+} (Figs. 4G and 5G). SO_4^{2-} and HCO_3^- are not plotted because they were below the limits of detection (~15 mmolal) for all Cretaceous fluid inclusions analyzed. The low concentrations of SO_4^{2-} and HCO_3^- in fluid inclusions show that the parent waters of these Cretaceous halites were enriched in Ca^{2+}, with equivalents $Ca^{2+} > SO_4^{2-} + HCO_3^-$. Such enrichment in Ca^{2+} indicates that after evaporation and precipitation of calcium carbonate and gypsum, Ca^{2+} but not SO_4^{2-} or HCO_3^- remained in the brines. Curves that track the compositional paths predicted for equilibrium evaporation of modern seawater calculated with the HMW computer model at 25 °C are plotted on Figs. 4 and 5. Curves are also plotted that simulate evaporation of Aptian seawater (Fig. 4) and Albian-Cenomanian seawater (Fig. 5), calculated with the HMW computer program (see below). Salts formed during simulated evaporation of Aptian and Albian-Cenomanian seawater are shown as horizontal bars along the top of Figs. 4 and 5.

Fluid inclusions from halites that precipitated relatively early in the halite field, before crystallization of potash salts, and which define an evaporation path, are illustrated by closed symbols on Figs. 4 and 5. These fluid inclusions are probably the most representative of evaporated Cretaceous seawater and were used for calculations of Aptian and Albian-Cenomanian seawater compositions. Fluid inclusions represented by open symbols generally contain more concentrated brines, with some approaching saturation with the potash minerals sylvite and carnallite (Fig. 4). These more concentrated inclusion brines show greater scatter in chemical composition because they are more likely to have been influenced by processes other than evaporative concentration, for example, syndepositional recycling of potash salts. Such inclusions were not used for calculations of Cretaceous seawater compositions.

Thirteen of fourteen fluid inclusions from the lower chevron halite interval (792 m), Sergipe basin, contain less evolved brines, whereas seven fluid inclusions from overlying chevron halites (768 m) are more scattered in chemical composition, with some highly concentrated brines at or near sylvite and carnallite saturation (Table 2a, Fig. 4). The Sergipe basin fluid inclusions from halite at 792 m are probably most representative of evaporated Aptian seawater because of their stratigraphic position at the base of the evaporite section, and because their chemistries indicate precipitation early in the halite field.

Most brine inclusions in halite from the Congo basin are of the highly evolved type, consistent with their stratigraphic position in the upper Loeme Formation (Table 2b, Figs. 2B and 4). Congo basin fluid inclusions are generally rich in Ca^{2+}, Mg^{2+}, and Cl^-, and depleted in K^+ and Na^+, some with compositions in the potash salt precipitation fields. None of the Congo basin fluid inclusions appear to be representative of pristine Aptian evaporated seawater and so are not used for Cretaceous seawater modeling calculations.

All fluid inclusions from the Khorat Plateau come from halites near the base of the Lower Halite Member of the Maha Sarakham Formation. The Br^- profile (Fig. 3B) indicates that all seven stratigraphic intervals sampled contain halites with less than 100 ppm Br^-, that is, halites formed relatively early in the halite precipitation field. These fluid inclusions therefore likely contain uncontaminated samples of evaporated Albian-Cenomanian seawater. Most Maha Sarakham Formation fluid inclusions plot along well-defined trends that lie at the beginning of the halite facies of the evaporation path. Near the base of the halite section (430.5 and 428 m), however, many brine inclusions contain anomalously low K^+ concentrations, generally less than 200 mmolal (Figs. 5D, F, and G). Those inclusions show more scatter on the ion–ion plots and they do not lie along the evaporation curves defined by the Maha Sarakham fluid inclusions; they are given open symbols on Fig. 5 and were not used for calculation of Albian-Cenomanian seawater chemistry. The reasons for the low K^+ concentrations in fluid inclusions from halites in the lowermost part of the Maha Sarakham stratigraphic section are not known.

The concentrations of Na^+ versus Cl^- in fluid inclusions from all three Cretaceous halites lie along well-defined curves clearly different from the evaporation path of modern seawater (Figs. 4A and 5A). At the point of halite saturation (~6300 mmolal Cl^-), the concentration of Na^+ decreases; Cl^- molalities increase during further evaporative concentration, which is the behavior exhibited by ion pairs where the initial molality of $Cl^- > Na^+$. The Cretaceous fluid inclusions fall along the halite precipitation segments of the evaporation curves, as expected, but the concentrations of Cl^- are higher than those produced during the evaporation of present-day seawater, and the concentrations of Na^+ are lower. That trend shows that the Cretaceous parent waters had a lower Na^+/Cl^- ratio than modern seawater.

Cretaceous fluid inclusions are depleted in Mg^{2+} compared to the brines produced during evaporation of

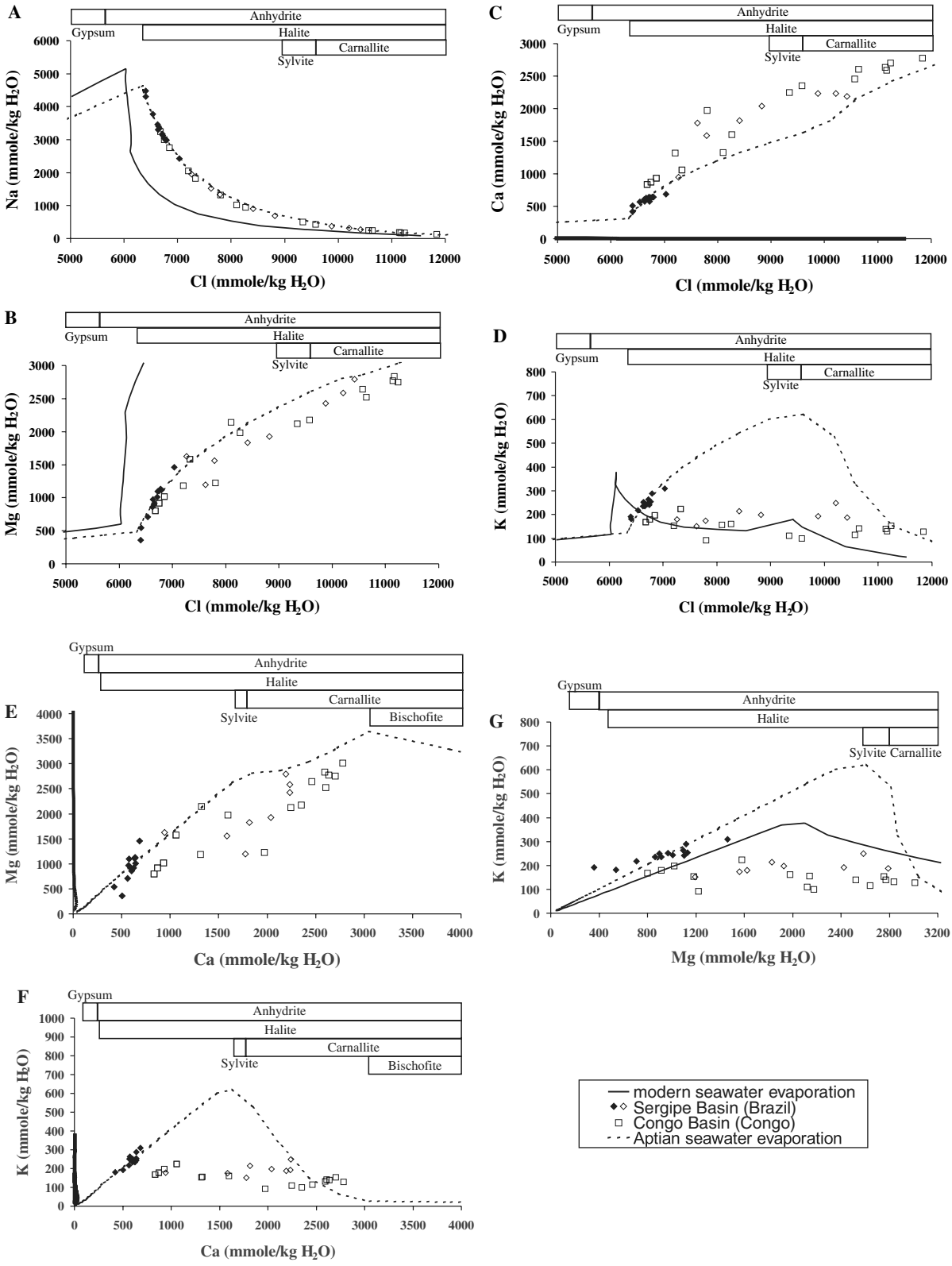

Fig. 4. Chemical analyses of Cretaceous fluid inclusions in halite from the Sergipe and Congo basins. Solid symbols for Sergipe basin represent individual fluid inclusions with chemical compositions diagnostic of halite precipitation early in the halite "facies" before crystallization of any late-stage potash salts. Fluid inclusions with open symbols from the Sergipe and Congo basins contain more concentrated brines, some approaching and exceeding saturation with the potash minerals sylvite and carnallite. Such concentrated fluid inclusion brines are more scattered in chemical composition and more likely to have undergone syndepositional chemical modifications by recycling with earlier formed brines or potash salts. Solid curves trace the paths calculated for equilibrium evaporation of modern seawater simulated with the HMW computer program at 25 °C. Dashed curves track the evaporation of Aptian seawater (121.0–112.2 Ma) simulated with the HMW computer program at 25 °C. Minerals predicted to precipitate during the evaporation of Aptian seawater are shown with horizontal bars.

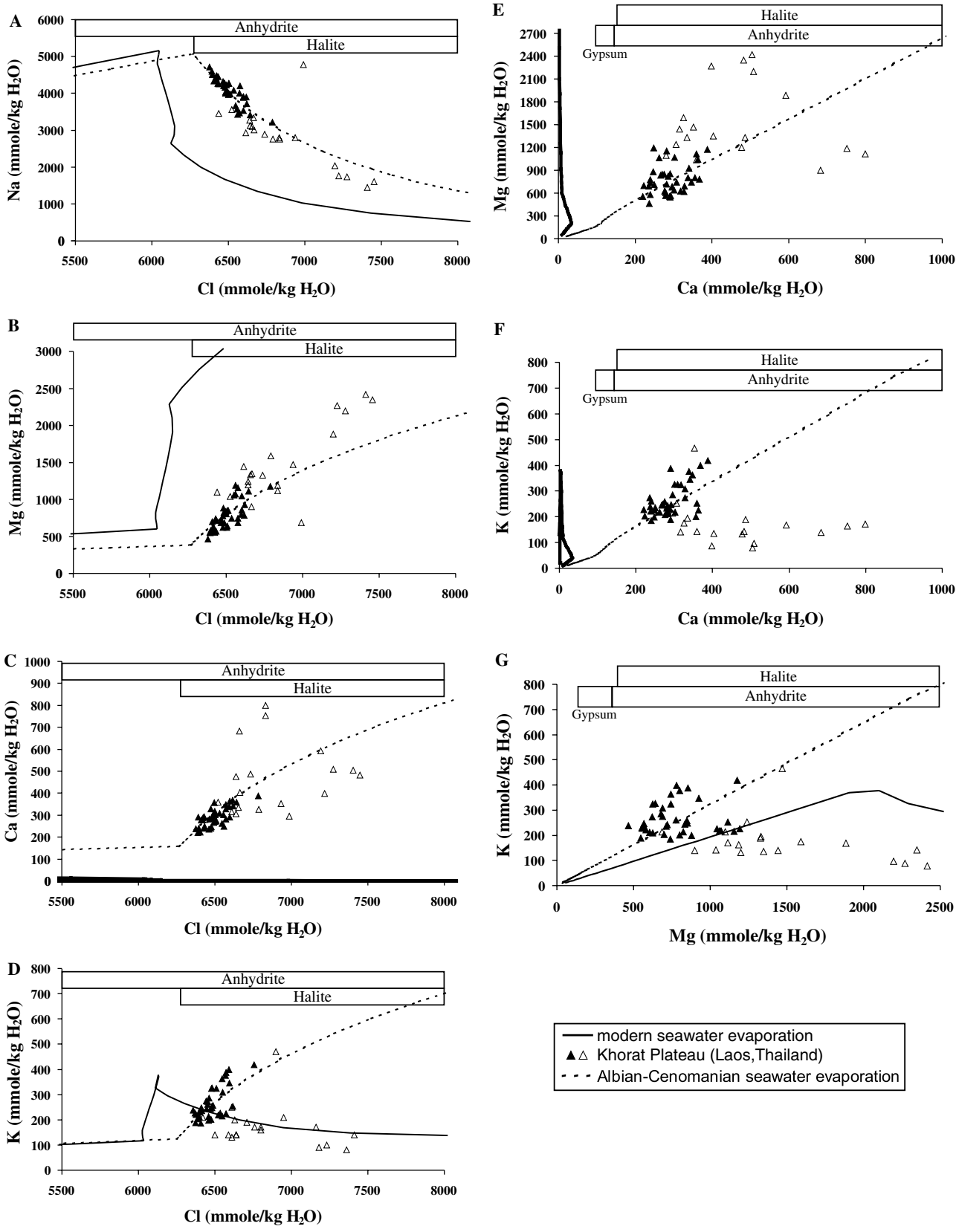

Fig. 5. Chemical analyses of Cretaceous individual fluid inclusions in halite from the Khorat Plateau, Laos, and Thailand. Solid symbols represent fluid inclusions with chemical compositions diagnostic of halite precipitation early in the halite "facies" before crystallization of potash salts. Fluid inclusions with open symbols contain more concentrated brines, which are more likely to have undergone syndepositional chemical modifications. Solid curves trace the paths calculated for equilibrium evaporation of modern seawater simulated with the HMW computer program at 25 °C. Dashed curves track the evaporation of Albian-Cenomanian seawater (112.2–93.5 Ma) simulated with the HMW computer program at 25 °C. Minerals predicted to precipitate during the evaporation of Albian-Cenomanian seawater are shown with horizontal bars.

modern seawater, as shown on plots of Mg^{2+} versus Cl^- (Figs. 4B and 5B). At the onset of halite precipitation, Mg^{2+} concentrations rise steeply because Cl^- is lost from the brines when halite forms. Mg^{2+} concentrations at halite saturation for all Cretaceous fluid inclusions are significantly lower than the Mg^{2+} concentrations at halite saturation during evaporation of modern seawater, which indicates the parent waters of these Cretaceous evaporites were depleted in Mg^{2+} relative to modern seawater, with a lower Mg^{2+}/Cl^- ratio. Some inclusions from the Congo and Sergipe basins contain highly concentrated brines, with elevated Mg^{2+} concentrations at or near saturation with respect to sylvite and carnallite.

Cretaceous brine inclusions are strikingly different from brines produced during evaporation of modern seawater as shown in the Ca^{2+} versus Cl^- plots (Figs. 4C and 5C). The concentration of Ca^{2+} drops to very low values during the evaporation of modern seawater because with $SO_4^{2-} > Ca^{2+}$, precipitation of $CaSO_4$ removes most of the Ca^{2+} from the brine before halite precipitates (Figs. 4 and 5C). In contrast, Cretaceous parent waters had $Ca^{2+} > SO_4^{2-}$; during precipitation of calcium sulfate, SO_4^{2-} was removed from the brine, leaving excess Ca^{2+} before halite saturation was reached. Without SO_4^{2-} in the brine, Ca^{2+} could become concentrated during further evaporation into the halite field because the next Ca-bearing mineral in the evaporation sequence is the highly soluble mineral tachyhydrite. High Ca^{2+} concentrations are common to all Cretaceous fluid inclusions. The most concentrated brine inclusions show the most scatter.

Early in the halite precipitation field, K^+ concentrations increase along well-defined evaporation curves for the Sergipe basin and Khorat Plateau fluid inclusions, illustrated by the K^+ versus Cl^- plots (Figs. 4D and 5D). Inclusions with highly concentrated brines from the Sergipe and Congo basins, and from the Khorat Plateau, have relatively low K^+ concentrations which do not fall along well-defined evaporation curves. The low K^+ concentrations in some Cretaceous fluid inclusions cannot be due to precipitation of K-sulfate salts because the Cretaceous brines contained no measurable SO_4^{2-}. K^+ concentrations during evaporation of modern seawater, for example, never exceed 400 mmolal because of precipitation of the K-sulfate-bearing mineral polyhalite (Table 1), which forms after halite. The first K-bearing salts to precipitate from Cretaceous brines, however, are sylvite and carnallite, which is shown on the simulated evaporation curves where K^+ begins to decrease (Fig. 4D).

Fluid inclusions in Cretaceous halites, with high concentrations of Ca^{2+} and Mg^{2+}, are quite different in composition from brines expected to form during the evaporation of modern seawater (Figs. 4E and 5E). The modern seawater evaporation curve is nearly vertical on these plots, with Ca^{2+} removed from the brines before halite precipitation. Cretaceous brines, on the other hand, lost almost all their SO_4^{2-} as $CaSO_4$ before halite precipitation. Therefore only minor amounts of $CaSO_4$ and no $MgSO_4$-bearing salts form in the halite field of the evaporation pathway, and plots of Mg^{2+} versus Ca^{2+} are nearly straight lines (Figs. 4E and 5E). Although there is scatter in the data, the Mg^{2+} versus Ca^{2+} plots show that the fluid inclusion chemical compositions from the Sergipe basin and Khorat Plateau cluster around straight lines defined by constant Mg^{2+}/Ca^{2+} ratios of 1.6 and 2.7, respectively. These ratios are significant because they give direct information about the Mg^{2+}/Ca^{2+} ratios of the Cretaceous parent waters (Table 3). The above Mg^{2+}/Ca^{2+} ratios are maxima, because some Ca^{2+} was lost earlier in the evaporation sequence during precipitation of carbonates and $CaSO_4$.

Additional differences between the Cretaceous inclusion brines with abundant Ca^{2+}, and brines formed during evaporation of modern seawater are illustrated on the K^+ versus Ca^{2+} plots (Figs. 4F and 5F). Less concentrated brines from the Sergipe basin and Khorat Plateau plot, with some scatter, along curves of constant K^+/Ca^{2+}, which reflects the conservative behavior of these ions during precipitation of halite, after the bulk of the $CaSO_4$ precipitated and before any K–Ca-bearing potash salts formed. Lines of constant K^+/Ca^{2+} give information on the K^+/Ca^{2+} of the Cretaceous parent waters; they are 0.4 and 0.9 for the Sergipe basin and Khorat Plateau, respectively (Table 3). Again, these K^+/Ca^{2+} ratios are maximum values, because Ca^{2+} was lost earlier in the evaporation sequence during precipitation of carbonates and $CaSO_4$ and no K-bearing salts are precipitated until the sylvite and carnallite fields are reached. The most concentrated brines from the Sergipe and Congo basins and the Khorat Plateau are relatively depleted in K^+ and plot below the lines of constant K^+/Ca^{2+} defined by the halite facies fluid inclusions.

The final plots, K^+ versus Mg^{2+} (Figs. 4G and 5G) show that Cretaceous fluid inclusion compositions lie along trends that differ from the evaporation pathway of modern seawater, where K^+ concentrations beyond halite saturation are controlled by the K-bearing salt polyhalite. Instead, K^+ and Mg^{2+} both exhibit conservative behavior

Table 3
Major-ion compositions of primary fluid inclusions (mmol/kg H_2O) in Cretaceous marine halites, as averages of brine inclusion data for each time period

Time	Age (Ma)	$m(Mg^{2+})/m(K^+)$	$m(Mg^{2+})/m(Ca^{2+})$	$m(K^+)/m(Ca^{2+})$	$m(Ca^{2+})$ excess[a]
Albian-Cenomanian	112.2–93.5	3.1	2.7	0.9	12
Aptian	121.0–112.2	3.8	1.6	0.4	27

[a] $m(Ca^{2+})$ excess is $m(Ca^{2+}) - m(SO_4^{2-})$ in initial seawater, in mmol/kg H_2O. Cretaceous $m(Ca^{2+})$ excess was obtained from average brine inclusion $m(K^+)/m(Ca^{2+})$ ratios, assuming Cretaceous seawater had $m(K^+) = 11$ mmol/kg H_2O (see text).

during evaporation in the halite facies; K^+ and Mg^{2+} concentrations are influenced late in the evaporation path by precipitation of sylvite and carnallite. The Sergipe basin and Khorat Plateau brine inclusions cluster, with scatter, along evaporation curves with constant Mg^{2+}/K^+ ratios. Significantly, these Mg^{2+}/K^+ values represent the original ratio of Mg^{2+}/K^+ of the unevaporated parent water (Table 3). The average Mg^{2+}/K^+ ratio in fluid inclusions from the Sergipe basin and Khorat Plateau, is 3.8 and 3.1, respectively, compared to the value of 5.2 in modern seawater.

In summary, the major-ion compositions of Cretaceous brine inclusions indicate that Cretaceous seawater was enriched in Ca^{2+} (Figs. 4C and 5C), depleted in SO_4^{2-}, Na^+ (Figs. 4A and 5A), and Mg^{2+} (Figs. 4B and 5B), and with lower Na^+/Cl^-, Mg^{2+}/Ca^{2+}, and Mg^{2+}/K^+ ratios, compared to brines formed during evaporation of present-day seawater. Aptian fluid inclusions are extremely enriched in Ca^{2+} with lower Mg^{2+}/Ca^{2+} ratios than Albian-Cenomanian brine inclusions indicating variations in the major-ion chemistry of seawater during the Cretaceous.

3.2. Calculation of major-ion chemistry of Cretaceous seawater

The major ion composition (Mg^{2+}, Ca^{2+}, Na^+, K^+, SO_4^{2-}, and Cl^-) of Cretaceous seawater is calculated from fluid inclusion chemistries and the HMW computer program. The HMW computer program is used to model Cretaceous seawater compositions that, when evaporated, best match the brine inclusion data from the Sergipe basin (Fig. 4) and the Khorat Plateau (Fig. 5). We calculate the chemical composition of Cretaceous seawater for the Aptian (121.0–112.2 Ma) and the Albian to Cenomanian (112.2–93.5 Ma) (Table 4).

We make the following assumptions, which are discussed more thoroughly in Lowenstein et al. (2005). (1) Cl^- concentration in the Cretaceous oceans was 565 mmolal, equal to present-day seawater. Although there is no direct information on the paleosalinity and chlorinity of Cretaceous seawater, fluid inclusions in Paleozoic marine calcite cements suggest that seawater salinity has not changed dramatically in the Phanerozoic (Johnson and Goldstein, 1993; Ward et al., 1993). (2) HCO_3^- is ignored in the calculations because its concentration in modern seawater (2.5 mmolal), and presumably Cretaceous seawater, is small compared to Cl^- (565 mmolal) and the other major ions. (3) The K^+ concentration in Cretaceous seawater is about the same as in modern seawater (11 mmolal). This assumption is based on the similar K^+/Br^- ratios in fluid inclusions in Silurian, Devonian, Permian, Triassic, and Miocene halites and the long residence time of Br^- in seawater of ~100 million years (Horita et al., 2002; Lowenstein et al., 2005).

The Mg^{2+}/K^+ ratio in Cretaceous seawater is measured directly from the chemical compositions of brine inclusions in halite because no K- or Mg-bearing salts form before halite in the evaporation sequence. Therefore the Mg^{2+}/K^+ ratios of the brine inclusions are the same as in Cretaceous seawater. The average Mg^{2+}/K^+ ratios for Aptian and Albian-Cenomanian seawater are 3.8 and 3.1, respectively (Table 3). Using a K^+ concentration of 11 mmolal gives Mg^{2+} concentrations of 42 and 34 mmolal in Cretaceous seawater, which are lower than the Mg^{2+} in modern seawater (55 mmolal) (Table 4).

The K^+/Ca^{2+} ratios measured from Cretaceous brine inclusions are used to calculate the Ca^{2+} of Cretaceous seawater. The average K^+/Ca^{2+} for Aptian and Albian-Cenomanian brine inclusions (Table 3) and the K^+ concentration of 11 mmolal give Ca^{2+} concentrations of 27 and 12 mmolal, respectively, for Aptian and Albian-Cenomanian seawater. This Ca^{2+} is the "excess" calcium after crystallization of $CaCO_3$ and $CaSO_4$ (Table 3); the actual concentration of Ca^{2+} in Cretaceous seawater must have been higher. In these calculations, the formation of carbonates is ignored because only ~10% of the Ca^{2+} in present day seawater is lost during precipitation of $CaCO_3$. To calculate the true concentration of Ca^{2+} in Cretaceous seawater, information is needed on the amount of SO_4^{2-} in Cretaceous seawater that was presumably consumed as $CaSO_4$ prior to halite precipitation. SO_4^{2-} was below detection in the Cretaceous brine inclusions so its concentration in Cretaceous seawater must be estimated. Horita et al. (2002) and Lowenstein et al. (2003, 2005) assume the concentration product of $(Ca^{2+})(SO_4^{2-})$ in ancient seawater ranged from 150 to 450 mmolal^2 (0.5 to 1.5 the value of 319 mmolal^2 in present day seawater). Although there are no data to validate this assumption, this concentration product constraint is consistent with available information on seawater salinities in the Phanerozoic (Johnson and Goldstein, 1993; Ward et al., 1993) and is well below the

Table 4
Major-ion chemistry of Cretaceous seawater (mmol/kg H_2O) calculated from chemical composition of fluid inclusions in marine halite[a]

Time	Age (Ma)	$m(Na^+)$	$m(K^+)$	$m(Ca^{2+})$	$m(Mg^{2+})$	$m(Cl^-)$	$m(SO_4^{2-})$	$m(Mg^{2+})/m(Ca^{2+})$
Modern seawater	0	485	11	11	55	565	29	5.2
Albian-Cenomanian	112.2–93.5	462	11	26 (20–28)	34	565	14 (8–16)	1.3 (1.2–1.7)
Aptian	121.0–112.2	416	11	35.5 (32–39)	42	565	8.5 (5–12)	1.2 (1.1–1.3)

[a] $m(Cl^-)$ is assumed to be equal to modern seawater. $m(K^+)$ is assumed to be equal to 11 mmol/kg H_2O (Horita et al., 2002). $m(Mg^{2+})$ is estimated from $m(K^+)$ of Cretaceous seawater and average ratio of $m(Mg^{2+})/m(K^+)$ in brine inclusions (Table 3). $m(Ca^{2+})$ and (SO_4^{2-}) are obtained from $m(Ca^{2+})$ excess (Table 3) and assumption that the concentration product of $(Ca^{2+})(SO_4^{2-})$ in Cretaceous seawater was equal to the modern seawater value of 300 mmolal^2 or had a range between 150 and 450 mmolal^2, in parentheses. $m(Na^+)$ in Cretaceous seawater is calculated by charge balance, after concentrations of all other ions (Cl^-, SO_4^{2-}, Ca^{2+}, Mg^{2+}, and K^+) are estimated.

product at gypsum saturation, $(Ca^{2+})(SO_4^{2-}) > 3000$ mmolal^2 (Lowenstein et al., 2005). Aptian seawater, with a Ca^{2+} excess of 27 mmolal and using the $(Ca^{2+})(SO_4^{2-})$ concentration product assumption, has $Ca^{2+} = 32$ mmolal, $SO_4^{2-} = 5$ mmolal, and $(Ca^{2+})(SO_4^{2-}) = 160$ mmolal^2 as a lower limit. As an upper limit, $Ca^{2+} = 39$ mmolal, $SO_4^{2-} = 12$ mmolal, and $(Ca^{2+})(SO_4^{2-}) = 468$ mmolal^2. If the $(Ca^{2+})(SO_4^{2-})$ were the same as in present-day seawater ($\sim$300 mmolal^2), Aptian seawater has $Ca^{2+} = 35.5$ mmolal and $SO_4^{2-} = 8.5$ mmolal. Using the same procedure, Albian-Cenomanian seawater, with Ca^{2+} excess of 12 mmolal (Table 3), has $Ca^{2+} = 26$ mmolal and $SO_4^{2-} = 14$ mmolal, with a range of $Ca^{2+} = 20$–28 mmolal and $SO_4^{2-} = 8$–16 mmolal. Clearly, Cretaceous seawater has much higher concentrations of Ca^{2+}(>20 mmolal) than modern seawater (11 mmolal), no matter what assumptions are made about the concentration of SO_4^{2-} in the Cretaceous oceans. Extremely high concentrations of Ca^{2+} in Aptian seawater, more than three times that in modern seawater, dropped to lower, but still relatively high values in the Albian-Cenomanian (Table 4).

Na^+ in Cretaceous seawater is calculated by charge balance, after all other major ion concentrations are calculated. Na^+ concentrations in the Aptian (416 mmolal) and Albian-Cenomanian (462 mmolal) are lower than the Na^+ measured from present day seawater (485 mmolal) (Table 4).

Earlier published estimates of Aptian and Albian-Cenomanian seawater chemistry used slightly different assumptions to compute the Mg^{2+}/Ca^{2+} ratios of Cretaceous seawater (Lowenstein et al., 2001). In that publication, maximum Mg^{2+}/Ca^{2+} ratios of 1.6 and 2.3 for Aptian and Albian-Cenomanian seawater, respectively, were given on the basis of direct measurements of Mg^{2+} and Ca^{2+} from fluid inclusions. Those ratios, however, did not account for the Ca^{2+} lost from seawater during earlier precipitation of $CaCO_3$ and $CaSO_4$, formed before halite. Lower limits of the Mg^{2+}/Ca^{2+} ratio (1.1 and 1.4 for Aptian and Albian-Cenomanian seawater, respectively) were calculated by Lowenstein et al. (2001) assuming Cretaceous seawater had SO_4^{2-} of 14 mmol, about half the concentration of sulfate in modern seawater. Here, we followed the convention of Horita et al. (2002) and Lowenstein et al. (2003, 2005) and assume the concentration product of $(Ca^{2+})(SO_4^{2-})$ in ancient seawater ranged from 150 to 450 mmolal^2 (0.5 to 1.5 the value of 319 mmolal^2 in present day seawater). In addition, more fluid inclusions, particularly from the Albian-Cenomanian Maha Sarakham Formation, were used to calculate the paleoseawater compositions reported here. The result of the additional data and consistent treatment of SO_4^{2-} is a slightly lower Mg^{2+}/Ca^{2+} ratio for Albian-Cenomanian seawater (1.2–1.7, Table 4) than the ratio of 1.4–2.3 reported in Lowenstein et al. (2001).

Estimates of the concentrations of Ca^{2+} and SO_4^{2-} in Cretaceous seawater, calculated using the same assumptions reported here, were presented in Lowenstein et al. (2003, Fig. 1 and Table DR1). Their Aptian seawater Ca^{2+} and SO_4^{2-} concentrations are the same as given here. Albian-Cenomanian Ca^{2+} and SO_4^{2-} seawater concentrations have been slightly revised because of additional fluid inclusion analyses from the Maha Sarakham Formation after publication of Lowenstein et al. (2003).

4. Discussion and conclusions

Cretaceous seawater was relatively enriched in Ca^{2+} and depleted in Mg^{2+}, Na^+, and SO_4^{2-} compared to present-day seawater. Elevated Ca^{2+} concentrations, with $Ca^{2+} > SO_4^{2-}$ at the point of gypsum saturation, allowed Cretaceous seawater to evolve into Mg^{2+}–Ca^{2+}–Na^+–K^+–Cl^- brines lacking measurable SO_4^{2-}. High calcium concentrations also give Cretaceous seawater the lowest Mg^{2+}/Ca^{2+} ratios ($\sim$1) so far documented in Phanerozoic seawater from fluid inclusions in halite (Lowenstein et al., 2003, 2005), and within the range chemically favorable for precipitation of low-Mg calcite ooids and cements. Early Cretaceous (Aptian) seawater was extreme in its Ca^{2+} enrichment, more than three times higher than present day seawater, with an estimated Mg^{2+}/Ca^{2+} ratio of 1.1–1.3. Later (Albian-Cenomanian) seawater had somewhat lower Ca^{2+}, and a higher Mg^{2+}/Ca^{2+} ratio of 1.2–1.7 (Table 4). Similarly low Mg^{2+}/Ca^{2+} ratios, 1.7–1.8 and 0.9, have been estimated for Hauterivian (130 Ma) and Albian (100 Ma) seawater, respectively, from echinoderm calcite (Table 5) (Dickson, 2002, 2004). Cretaceous (Albian) echinoderms give the lowest seawater Mg^{2+}/Ca^{2+} ratio (0.9) in the Phanerozoic (Dickson, 2004). Estimates of Cretaceous seawater Mg^{2+}/Ca^{2+} ratios from rudist calcite also give low values (Table 5), although Lower Campanian (81.4 Ma) rudists apparently indicate higher seawater Mg^{2+}/Ca^{2+} ratios, between 2.7 and 3.5 (Steuber and Rauch, 2005). The lowest rudist-derived paleoseawater Mg^{2+}/Ca^{2+} ratio (0.8–1.3) comes from Middle Albian (106.0 Ma) samples (Steuber and Rauch, 2005). These results from halite fluid inclusions and echinoderm and rudist calcite all indicate that Early Cretaceous seawater (Hauterivian, Barremian, Aptian, and Albian) had lower Mg^{2+}/Ca^{2+} ratios than Late Cretaceous seawater (Coniacian, Santonian, and Campanian) (Fig. 6A).

The good textural preservation of primary calcite oolites suggests that the Cretaceous oceans were "calcite seas", different from the "aragonite facilitating" conditions of modern oceans (Sandberg, 1983; Wilkinson et al., 1985). Although there has been debate on the causes of calcite seas versus aragonite seas, one explanation involves changes in the chemistry of seawater, specifically lowering of the Mg^{2+}/Ca^{2+} ratio to values below two (Hardie, 1996; Stanley and Hardie, 1998). The Mg^{2+}/Ca^{2+} ratio of $\sim$2 is the chemical divide separating waters in which low Mg-calcite precipitates ($Mg^{2+}/Ca^{2+} < 2$) from those in which aragonite $\pm$ high Mg-calcite are predicted to form (Füchtbauer and Hardie, 1976; Hardie,

Table 5
Estimated Mg^{2+}/Ca^{2+} ratios of Cretaceous seawater

Mg^{2+}/Ca^{2+}	Stage	Age (Ma)	Source	Reference
2.7–3.5	Lower Campanian	81.4	Rudist calcite	Steuber and Rauch (2005)
1.6–2.2	Upper Santonian	84.8	Rudist calcite	Steuber and Rauch (2005)
1.9–2.9	Coniacian	88.2	Rudist calcite	Steuber and Rauch (2005)
1.5–2.1	Middle Cenomanian	96.0	Rudist calcite	Steuber and Rauch (2005)
1.2–1.7	Albian-Cenomanian	112.2–93.5	Halite fluid inclusions	This study
0.9	Albian	100	Echinoderm calcite	Dickson (2004)
0.8–1.3	Middle Albian	106.0	Rudist calcite	Steuber and Rauch (2005)
1.1–1.3	Aptian	121.0–112.2	Halite fluid inclusions	This study
0.9–1.4	Upper Barremian	121.2	Rudist calcite	Steuber and Rauch (2005)
1.7–1.8	Hauterivian	130	Echinoderm calcite	Dickson (2004)

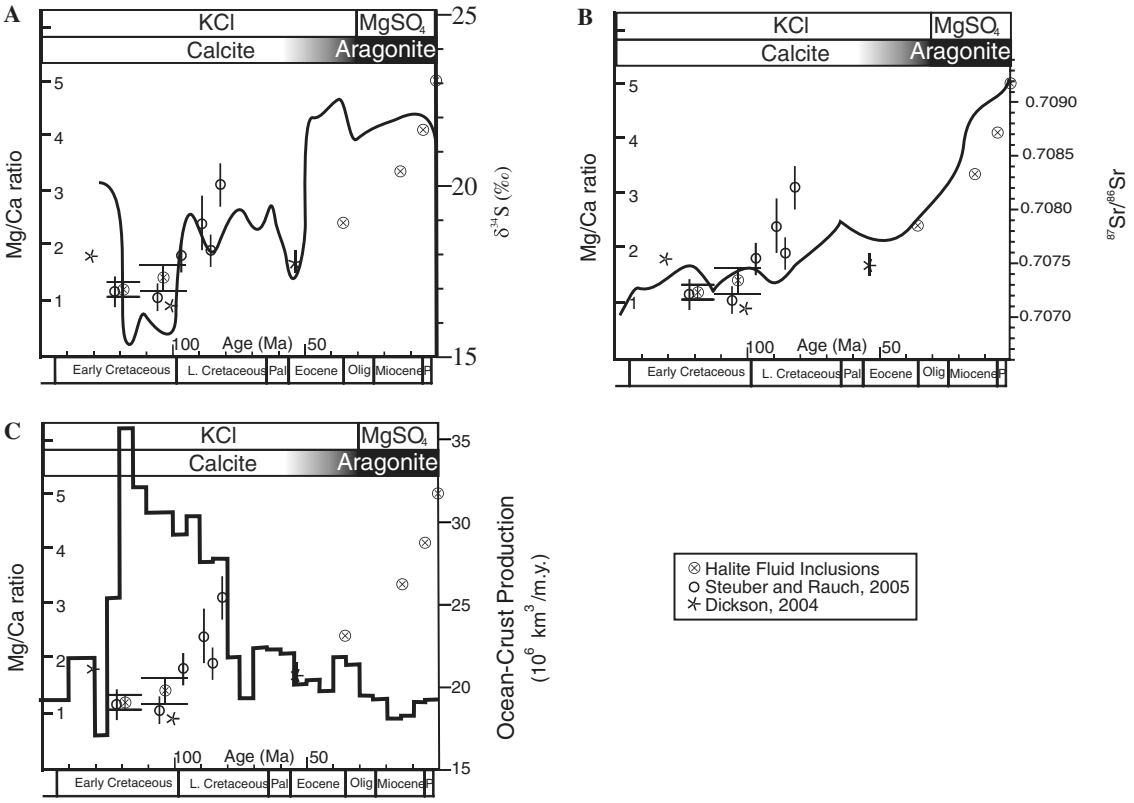

Fig. 6. Secular variations in the Mg^{2+}/Ca^{2+} ratios of seawater over the past 130 Ma, estimated from fluid inclusions in halite (this paper, and with Paleogene/Neogene values from Lowenstein et al., 2001), echinoderms (Dickson, 2004), and rudists (Steuber and Rauch, 2005). Temporal trends in the primary mineralogies of nonskeletal carbonates and KCl–$MgSO_4$ evaporites are modified from Sandberg (1983) and Hardie (1996), respectively. (A) Sulfur isotope curve ($\delta^{34}S_{SO_4}$) from marine barites, modified from Paytan et al. (2004). (B) Seawater $^{87}Sr/^{86}Sr$ curve, modified from Jones and Jenkyns (2001). (C) Ocean crust production curve modified from Larson (1991).

1996). The results from this study confirm that the very low Mg^{2+}/Ca^{2+} in Cretaceous seawater was responsible for calcite being the nonskeletal marine carbonate of that time. These very low Mg^{2+}/Ca^{2+} ratios are also consistent with the generally higher temperatures inferred for the Cretaceous oceans. Temperature exerts a strong control on precipitation of nonskeletal marine carbonates, with aragonite favored at higher temperatures and calcite at lower temperatures (Burton and Walter, 1987; Morse et al., 1997). In order for calcite to precipitate at temperatures of 20 °C, for example, seawater must have a Mg^{2+}/Ca^{2+} ratio of ~1 (Morse et al., 1997, Fig. 1). At 30 °C, calcite only forms at Mg^{2+}/Ca^{2+} ratio of <1 (Morse et al., 1997). The enigma of finding the low temperature carbonate mineral, calcite, in limestones interpreted to have been deposited during warm climate periods like the Cretaceous may be explained by a shift in the Mg^{2+}/Ca^{2+} ratio of seawater to values of ~1. Apparently, the primary calcite formed in the warm Cretaceous oceans because the Mg^{2+}/Ca^{2+} ratio of seawater was low enough to cancel the influence of temperature favoring precipitation of aragonite (Morse et al., 1997).

Stanley and Hardie (1998) explored the relationship between seawater chemistry and the carbonate mineralogy of "dominant" reef builders and sediment-producing organisms (aragonite versus calcite). They interpreted changes in biomineralization patterns as the response of the biosphere to secular changes in the chemistry of seawater, specifically the Mg^{2+}/Ca^{2+} ratio and the concentration of Ca^{2+}. For the Cretaceous, they hypothesize that displacement of aragonitic hermatypic corals by rudists (calcite shell) as the dominant carbonate producers on carbonate platforms by the Turonian (Steuber, 2002), could have been caused by a decrease in the Mg^{2+}/Ca^{2+} ratio of seawater, as documented here. All Cretaceous sponges were calcitic, in contrast to modern aragonite seas in which calcisponges and demosponges secrete aragonite, high Mg-calcite, or both (Stanley and Hardie, 1998). Similarly, cheilostome bryozoans, which arose in the Cretaceous, precipitated calcite, whereas modern cheilostomes secrete aragonite and high Mg-calcite (Stanley and Hardie, 1998). Finally, the widespread deposition of massive calcite coccolith chalks in the Late Cretaceous may have been influenced by the low Mg^{2+}/Ca^{2+} ratio and high Ca^{2+} concentrations of Cretaceous seawater (Stanley and Hardie, 1998). Recent work on modern shell-building organisms (coralline algae, echinoids, crabs, shrimps, and calcareous serpulid worms) shows that the Mg^{2+}/Ca^{2+} ratio of seawater strongly influences the amount of Mg^{2+} incorporated into skeletal calcite, to the point that organisms may precipitate low-Mg calcite (<4 mole % $MgCO_3$) from waters with sufficiently low Mg^{2+}/Ca^{2+} ratios such as Cretaceous seawater (Stanley et al., 2002; Ries, 2004). These experimental studies lend further support to the link between seawater chemistry and temporal patterns of biomineralization. The results from this study suggest that the low Mg^{2+}/Ca^{2+} ratio of Cretaceous seawater favored carbonate producers on carbonate platforms that used calcite for shell construction.

Trends in Cretaceous seawater chemistry compare closely with records of marine S isotopes (Paytan et al., 2004), Sr isotopes (Jones and Jenkyns, 2001), as well as estimates of ocean crust production (Larson, 1991) (Figs. 6A–C). Generally light sulfur isotope values ($\delta^{34}S_{SO_4}$ below +19‰ in marine barite) in the Cretaceous compared to the past 45 m.y. have been attributed to higher global volcanic and midocean ridge hydrothermal activities, although other explanations, such as increased continental weathering inputs, are also possible (Paytan et al., 2004). Specifically, excursions to very low $\delta^{34}S_{SO_4}$ values during the Barremian-Aptian (~130–120 Ma) (Paytan et al., 2004) generally match the very low Mg^{2+}/Ca^{2+} ratios of seawater of that age (Table 5, Fig. 6A). Low $\delta^{34}S_{SO_4}$ values between 120 and 100 Ma agree with equally low Mg^{2+}/Ca^{2+} ratios in Aptian-Albian seawater. The rise in $\delta^{34}S_{SO_4}$ values between 100 and 95 Ma and the generally higher values in the Late Cretaceous parallel the rise of seawater Mg^{2+}/Ca^{2+} ratios to values above ~2 in the Late Cretaceous. Low seawater Mg^{2+}/Ca^{2+} ratios and $\delta^{34}S_{SO_4}$ values in the Early Cretaceous (Barremian-Albian) and the rise in both later in the Cretaceous suggest secular variations in the major ion chemistry and sulfur isotopes of seawater are related and may have a common cause.

Seawater $^{87}Sr/^{86}Sr$ ratios are low in the Cretaceous, in particular the Aptian-Albian negative excursion from ~121 to 98.9 Ma (Jones and Jenkyns, 2001), which parallels the low $\delta^{34}S_{SO_4}$ values and low seawater Mg^{2+}/Ca^{2+} ratios in the Aptian-Albian (Fig. 6B). Jones and Jenkyns (2001) modeled this negative seawater $^{87}Sr/^{86}Sr$ excursion using decreased river flux of Sr, decreased $^{87}Sr/^{86}Sr$ ratios in river inputs, or increased seafloor hydrothermal activity linked to increased ocean crust production at the MORs. Greater ocean crust production and seafloor hydrothermal activity during the Aptian-Albian is the interpretation most consistent with geologic data (see below; Jones and Jenkyns, 2001). It is also consistent with the low Mg^{2+}/Ca^{2+} ratios in Aptian-Albian seawater because the ocean crust through which hydrothermal brines circulate at the MORs is a source of Ca^{2+} and a sink for Mg^{2+}.

Ocean crust production plots for the Cretaceous, between 125 and 80 Ma, indicate an increase of 50–100% over modern rates (Fig. 6C; Larson, 1991). The most striking increase of ocean crust production is during the Barremian-Aptian "volcanic pulse" between 126 and 112 Ma, purported to be the largest igneous event on Earth in the past 160 m.y. (Larson and Erba, 1999). The high rates of ocean crust production during the Barremian-Aptian (Early Cretaceous) coincide with very low seawater Mg^{2+}/Ca^{2+} ratios in the Barremian-Albian. Late Cretaceous decreases in ocean crust production are matched by rising seawater Mg^{2+}/Ca^{2+} ratios between ~100 and 80 Ma, although no Mg^{2+}/Ca^{2+} data exist for the last 15 m.y. of the Cretaceous. The correspondence between high ocean crust production rates and low seawater Mg^{2+}/Ca^{2+} ratios in the Cretaceous suggests secular variations in the major ion chemistry of seawater may be related to variations in the flux of MOR hydrothermal brine driven by changes in the rate of ocean crust production, as postulated by Hardie (1996). Although variable ocean crust production rates are now debated, and indeed steady-state production of ocean crust over the past 180 m.y. has been advocated by Rowley (2002), the analysis by Demicco (2004) shows that relatively high ocean crust production rates are possible, indeed likely, for the Cretaceous.

In summary, the very low Mg^{2+}/Ca^{2+} seawater ratios during the Aptian-Albian, together with the Aptian-Albian negative excursion of $^{87}Sr/^{86}Sr$ ratios and $\delta^{34}S_{SO_4}$, and peak Cretaceous ocean crust production suggest a common cause, increased flux of MOR hydrothermal brine driven by an increase in the rate of ocean crust production, as proposed by Hardie (1996). Hardie (1996) predicted the observed fluctuations in Phanerozoic seawater chemistry to first order, modeling the major-ion composition of seawater by mixing MOR hydrothermal brine and river water (RW) inflows. Secular changes in seawater chemistry in the Hardie model are controlled by variations in the MOR/RW flux

ratio driven by changes in the rate of MOR crust production. MOR activity involves circulation of hot seawater through oceanic basalts and during this process, Na^+, Mg^{2+}, and SO_4^{2-} are exchanged from seawater to oceanic rocks and Ca^{2+} and K^+ are lost from basalts to seawater.

Hardie's predicted Cretaceous seawater generally matches the chemical compositions of Cretaceous seawater found in this study, that is, relative to modern seawater, Cretaceous seawater was enriched in Ca^{2+} and depleted in Na^+, Mg^{2+}, and SO_4^{2-}. The Cretaceous seawater Mg^{2+}/Ca^{2+} ratio of ~1 estimated by Hardie (1996) is close to the values for Cretaceous seawater (1.2 and 1.3 for Aptian and Albian-Cenomanian seawater, respectively) found in this study. Hardie (1996) estimated that K^+ was significantly elevated in Cretaceous seawater compared to modern seawater K^+ concentrations and to the calculated K^+ concentrations of this and other studies (Horita et al., 2002). To explain this discrepancy and the nearly constant concentrations of K^+ in Phanerozoic seawater, a sink is needed to take up K^+ coming from riverine and MOR inputs. The most likely K^+ sink is precipitation of K-bearing clay minerals during alteration of basalts in low-temperature off-axis areas of the MORs. K-bearing clays are known to form during off-axis "low" temperature (25–60 °C) hydrothermal alteration of basaltic crust (Wheat and Mottl, 2000) and across the seafloor in general (Schramm et al., 2005).

A recent extension of the Hardie (1996) model also produces seawater by mixing midocean ridge and river water inflows (Demicco et al., 2005). Demicco et al. (2005) however, add two important variables to the model: variable river water influx and cooler off-axis inflow waters that have chemically interacted with basalts. The study showed that cycling of seawater through the global midocean ridge system is required to model the evolution of ancient seawater. The off-axis flux is required as a K^+ sink in the model; variable river water fluxes produced the best matches with ancient seawater chemistries (Demicco et al., 2005).

Other explanations for the observed secular variations in the major-ion chemistry of ancient seawater do not involve changes in the rate of MOR crust production. Holland and Zimmermann (2000) and Holland (2005), for example, propose that global deceases in the rate of dolomite formation over the past 150 m.y. and the deposition of $CaSO_4$ evaporites during periods of high sea level may explain observed variations in seawater chemistry (decrease in Ca^{2+} concentration and increase in Mg^{2+} and SO_4^{2-} concentrations). Turchyn and Schrag (2004) suggest that the SO_4^{2-} concentration in seawater may be controlled by sulfate reduction and sulfide re-oxidation on continental shelves and slopes. These and other factors, such as variable riverine inputs (Berner, 2004), may contribute to producing the observed oscillations in the major-ion chemistry of seawater.

Other models address variations in the major ion chemistry of seawater using the coupled ocean-atmosphere reservoir flux approach of the "GEOCARB" family of models and the global cycles of sulfur and carbon (Wallmann, 2001; Hansen and Wallmann, 2003; Berner, 2004). Berner's (2004) model closely matches the calculated concentrations of Ca^{2+}, SO_4^{2-}, and the Mg^{2+}/Ca^{2+} ratio of seawater for the Phanerozoic (Lowenstein et al., 2001, 2003; Horita et al., 2002). The modeling illustrates the importance of Ca–Mg exchange (either by hydrothermal circulation of seawater at the MORs or by dolomitization of limestone) and secular variations in the rates of burial of pyrite and $CaSO_4$ versus weathering of pyrite and $CaSO_4$ (Berner, 2004).

Finally, cyclic changes in seawater chemistry and ocean crust production rates do not appear to coincide with global climate changes (icehouse/greenhouse oscillations) during the Cretaceous. It is becoming clear that the middle and late Cretaceous were warm greenhouse periods, whereas the early Cretaceous was a cooler episode (Huber, 1998; Tarduno et al., 1998; Jenkyns et al., 2004; Steuber et al., 2005). If global tectonism and the release of CO_2 are a primary influence on climate, then the early Cretaceous, the Barremian-Aptian volcanic pulse between 126 and 112 Ma, should correspond to a hothouse climate period. Yet, Steuber et al. (2005) show quite the opposite, that $\delta^{18}O$ values from rudist bivalves indicate the Barremian-Aptian was a relatively cool climatic interval. Although the Mg^{2+}/Ca^{2+} ratio of Cretaceous seawater appears to be linked to ocean crust production rates (Fig. 6C), Cretaceous climate does not.

Acknowledgments

Halite samples from the Khorat Plateau of Laos, along with geologic data, were kindly given by Robert Hite, U.S. Geological Survey. Thomas Steuber supplied data on rudist Mg^{2+}/Ca^{2+} ratios. Thanks to Bill Blackburn for maintaining the Environmental SEM, and to Robert Demicco, Lawrie Hardie, and Sean Brennan for their interest in understanding ancient seawater chemistry. Thomas Steuber, Charlotte Schreiber, Volodymyr Kovalevych, and A.E. Juske Horita made many good suggestions in their reviews. This work was supported by NSF Grant EAR9725740. Acknowledgment is made to the donors of the American Chemical Society Petroleum Research Fund for partial support of this research.

Associate editor: Juske Horita

References

Berner, R.A., 2004. A model for calcium, magnesium and sulfate in seawater over Phanerozoic time. *Am. J. Sci.* **304**, 438–453.

Burke, K., Sengor, A.M., 1988. Ten metre global sea-level change associated with South Atlantic Aptian salt deposition. *Mar. Geol.* **83**, 309–312.

Burton, E.A., Walter, L.M., 1987. Relative precipitation rates of aragonite and Mg-calcite from seawater: temperature or carbonate ion control? *Geology* **15**, 111–114.

Casas, E., Lowenstein, T.K., Spencer, R.J., Zhang, P., 1992. Carnallite mineralization in the nonmarine Qaidam basin, China: evidence for the

early diagenetic origin of potash evaporites. *J. Sediment. Petrol.* **62**, 881–898.

Coward, M.P., Purdy, E.G., Ries, A.C., Smith, D.G., 1999. The distribution of petroleum reserves in basins of the South Atlantic margins. In: Cameron, N.R., Bate, R.H., Clure, V.S. (Eds.), *The Oil and Gas Habitats of the South Atlantic*, vol. 153. Geological Society Special Publication, pp. 283–292.

de Ruiter, P.A.C., 1979. The Gabon and Congo Basins salt deposits. *Econ. Geol.* **74**, 419–431.

Demicco, R.V., 2004. Modeling seafloor-spreading rates through time. *Geology* **32**, 485–488.

Demicco, R.V., Lowenstein, T.K., Hardie, L.A., Spencer, R.J., 2005. Model of seawater composition for the Phanerozoic. *Geology* **33**, 877–880.

Dickson, J.A.D., 2002. Fossil echinoderms as monitor of the Mg/Ca ratio of Phanerozoic oceans. *Science* **298**, 1222–1224.

Dickson, J.A.D., 2004. Echinoderm skeleton preservation: calcite-aragonite seas and the Mg/Ca ratio of Phanerozoic oceans. *J. Sediment. Petrol.* **74**, 355–365.

El Tabakh, M., Utha-Aroon, C., Schreiber, B.C., 1999. Sedimentology of the Cretaceous Maha Sarakham evaporites in the Khorat Plateau of northeastern Thailand. *Sediment. Geol.* **123**, 31–62.

Evans, R., 1978. Origin and significance of evaporites in basins around Atlantic margin. *Am. Assoc. Petrol. Geol. Bull.* **62** (2), 223–234.

Fischer, A.G., 1980. Long-term climatic oscillations recorded in stratigraphy. In: *Climate in Earth History*. National Academy Press, pp. 97–104.

Füchtbauer, H., Hardie, L.A., 1976. Experimentally determined homogeneous distribution coefficients for precipitated magnesian calcites: application to marine carbonate cements (abstract). *Geol. Soc. Am. Abstr. Prog.* **8**, 877.

Hansen, K.W., Wallmann, K., 2003. Cretaceous and Cenozoic evolution of seawater composition, atmospheric O_2 and CO_2: a model perspective. *Am. J. Sci.* **303**, 94–148.

Hardie, L.A., 1996. Secular variation in seawater chemistry: an explanation for the coupled secular variation in the mineralogies of marine limestones and potash evaporites over the past 600 my. *Geology* **24**, 279–283.

Hardie, L.A., Lowenstein, T.K., Spencer, R.J., 1985. The problem of distinguishing between primary and secondary features in evaporites. In: Schreiber, B.C., Harner, H.L. (Eds.), *Sixth International Symposium on Salt*. Salt Institute, pp. 11–38.

Harris, N.B., 2000. Evolution of the Congo rift basin, west Africa: an inorganic geochemical record in lacustrine shales. *Basin Res.* **12**, 425–445.

Harvie, C.E., Møller, N., Weare, J.H., 1984. The prediction of mineral solubilities in natural waters: the Na-K-Mg-Ca-H-Cl-SO_4-OH-HCO_3-CO_3-CO_2-H_2O system to high ionic strengths at 25 °C. *Geochim. Cosmochim. Acta* **48**, 723–751.

Harvie, C.E., Weare, J.H., Hardie, L.A., Eugster, H.P., 1980. Evaporation of seawater: calculated mineral sequences. *Science* **208**, 498–500.

Hite, R.J., 1974. Evaporite deposits of the Khorat Plateau, northeastern Thailand. In: Coogan, A.H. (Ed.), *Fourth International Symposium on Salt*. Geological Society Northern Texas, pp. 135–146.

Hite, R.J., Japakesetr, T., 1979. Potash deposits of the Khorat Plateau, Thailand and Laos. *Econ. Geol.* **74**, 448–458.

Holland, H.D., 2005. Sea level, sediments and the composition of seawater. *Am. J. Sci.* **305**, 220–239.

Holland, H.D., Zimmermann, H., 2000. The dolomite problem revisited. *Int. Geol. Rev.* **42**, 481–490.

Holser, W.T., 1979. Trace elements and isotopes in evaporites. In: Burns, R.G. (Ed.), *Marine Minerals. Mineralogical Society of America Reviews in Mineralogy 6*. Mineralogical Society of America, pp. 295–346.

Horita, J., Zimmermann, H., Holland, H.D., 2002. The chemical evolution of seawater during the Phanerozoic: implications from the record of marine evaporites. *Geochim. Cosmochim. Acta* **66**, 3733–3756.

Huber, B.T., 1998. Tropical paradise at the Cretaceous poles? *Science* **282**, 2199–2200.

Jenkyns, H.C., Forster, A., Schouten, S., Damsté, J.S.S., 2004. High temperatures in the Late Cretaceous Arctic Ocean. *Nature* **432**, 888–892.

Johnson, W.J., Goldstein, R.H., 1993. Cambrian sea water preserved as inclusions in marine low-magnesium calcite cement. *Nature* **362**, 335–337.

Jones, C.E., Jenkyns, H.C., 2001. Seawater strontium isotopes, oceanic anoxic events, and seafloor hydrothermal activity in the Jurassic and Cretaceous. *Am. J. Sci.* **301**, 112–149.

Kovalevich, V.M., Peryt, T.M., Petrichenko, O.I., 1998. Secular variation in seawater chemistry during the Phanerozoic as indicated by brine inclusions in halite. *J. Geol.* **106**, 695–712.

Larson, R.L., 1991. Geological consequences of superplumes. *Geology* **19**, 963–966.

Larson, R.L., Erba, E., 1999. Onset of the mid-Cretaceous greenhouse in the Barremian-Aptian: igneous events and the biological, sedimentary, and geochemical responses. *Paleoceanography* **14**, 663–678.

Lowenstein, T.K., Hardie, L.A., 1985. Criteria for the recognition of salt-pan evaporites. *Sedimentology* **32**, 627–644.

Lowenstein, T.K., Hardie, L.A., Timofeeff, M.N., Demicco, R.V., 2003. Secular variation in seawater chemistry and the origin of calcium chloride basinal brines. *Geology* **31**, 857–860.

Lowenstein, T.K., Timofeeff, M.N., Brennan, S.T., Hardie, L.A., Demicco, R.V., 2001. Oscillations in Phanerozoic seawater chemistry: evidence from fluid inclusions in salt deposits. *Science* **294**, 1086–1088.

Lowenstein, T.K., Timofeeff, M.N., Kovalevych, V.M., Horita, J., 2005. The major-ion composition of Permian seawater. *Geochim. Cosmochim. Acta* **69**, 1701–1719.

Maurin, J.-C., Guiraud, R., 1993. Basement control in the development of the Early Cretaceous West and Central African rift system. *Tectonophysics* **228**, 81–95.

Morse, J.W., Wang, Q., Tsio, M.Y., 1997. Influences of temperature and Mg:Ca ratio on $CaCO_3$ precipitates from seawater. *Geology* **25**, 85–87.

Nürnberg, D., Müller, R.D., 1991. The tectonic evolution of the South Atlantic from Late Jurassic to present. *Tectonophysics* **191**, 27–53.

Oliver, F.Z. 1997. Sequência evaporitica Ibura da Bacia de Sergipe: Revisao de facies sedimentares, paleoambientes deposicionais e potencialidades na geracao de petroleo. Dissertacao de mestrado, Universidade Federal Fluminense. 145 pp.

Paytan, A., Kastner, M., Campbell, D., Thiemens, M.H., 2004. Seawater sulfur isotope fluctuations in the Cretaceous. *Science* **304**, 1663–1665.

Ries, J., 2004. Effect of ambient Mg/Ca ratio on Mg fractionation in calcareous marine invertebrates: a record of the oceanic Mg/Ca ratio over the Phanerozoic. *Geology* **32**, 981–984.

Rowley, D.B., 2002. Rate of plate creation and destruction: 180 Ma to present. *Geol. Soc. Am. Bull.* **114**, 927–933.

Sandberg, P.A., 1983. An oscillating trend in Phanerozoic nonskeletal carbonate mineralogy. *Nature* **305**, 19–22.

Sattayarak, N., Polachan, S., Charusirisawad, R. 1991. Cretaceous rock salt in the northeastern part of Thailand. (abstract). In: *Proceedings of the 7th Regional Conference Geology and Mineral Resources Southeast Asia (GEOSEA VII)*, Bangkok.

Schaller, H., 1969. Revisão estratigráfica da bacia de Sergipe/Alagoas. *Boletin Tecnico Petrobrás* **12** (1), 21–86.

Schramm, B., Devey, C.W., Gillis, K.M., Lackschewitz, K., 2005. Quantitative assessment of chemical and mineralogical changes due to progressive low-temperature alteration of East Pacific Rise basalts from 0 to 9 Ma. *Chem. Geol.* **218**, 281–313.

Silva, M.A.M. 1983. The Araripe Basin, northeastern Brazil: regional geology and facies analysis of a Lower Cretaceous evaporitic depositional complex. Ph.D. dissertation, Columbia University, 277 pp.

Smith, P.F.L., Stokes, R.B., Bristow, C., Carter, A., 1996. Mid-Cretaceous inversion in the northern Khorat Plateau of Lao PDR and Thailand. In: Hall, R., Blundell, D.J. (Eds.), *Tectonic Evolution of Southeast Asia*, 106. Geological Society of London Special Publication, pp. 233–246.

Stanley, S.M., Hardie, L.A., 1998. Secular oscillations in the carbonate mineralogy of reef-building and sediment-producing organisms driven by tectonically forced shifts in seawater chemistry. *Palaeogeogr. Palaeocl.* **144**, 3–19.

Stanley, S.M., Ries, J.B., Hardie, L.A., 2002. Low-magnesium calcite produced by coralline algae in seawater of Late Cretaceous composition. *Proc. Natl. Acad. Sci. USA* **99**, 15323–15326.

Steuber, T., 2002. Plate tectonic control on the evolution of Cretaceous platform-carbonate production. *Geology* **30**, 259–262.

Steuber, T., Rauch, M., 2005. Evolution of the Mg/Ca ratio of Cretaceous seawater: implications from the composition of biological low-Mg calcite. *Mar. Geol.* **217**, 199–213.

Steuber, T., Veizer, J., 2002. Phanerozoic record of plate tectonic control of seawater chemistry and carbonate sedimentation. *Geology* **30**, 1123–1126.

Steuber, T., Rauch, M., Masse, J., Graaf, J., Maloč, M., 2005. Low-latitude seasonality of Cretaceous temperatures in warm and cold episodes. *Nature* **437**, 1341–1344.

Szatmari, P., Carvalho, R.S., Simões, I.A., Tibana, P., Leite, D.C. 1974. Evaporitos de Sergipe. Geologia e geoquímica. Petrobras Projeto Evaporitos, vol. 1, 159 pp.

Szatmari, P., Carvalho, R.S., Simões, I.A., 1979. A comparison of evaporite facies in the Late Paleozoic Amazon and the Middle Cretaceous south Atlantic salt basins. *Econ. Geol.* **74**, 432–447.

Tarduno, J.A., Brinkman, D.B., Renne, P.R., Cottrell, R.D., Scher, H., Castillo, P., 1998. Evidence for extreme climatic warmth from Late Cretaceous Arctic vertebrates. *Science* **282**, 2241–2244.

Timofeeff, M.N., Lowenstein, T.K., Blackburn, W.H., 2000. ESEM-EDS: an improved technique for major element chemical analysis of fluid inclusions. *Chem. Geol.* **164**, 171–182.

Timofeeff, M.N., Lowenstein, T.K., Brennan, S.T., Demicco, R.V., Zimmermann, H., Horita, J., Von Borstel, L.E., 2001. Evaluating seawater chemistry from fluid inclusions in halite: examples from modern marine and nonmarine environments. *Geochim. Cosmochim. Acta* **65**, 2293–2300.

Turchyn, A., Schrag, D.P., 2004. Oxygen isotope constraints on the sulfur cycle over the past 10 million years. *Science* **303**, 2004–2007.

Utha-Aroon, C., 1993. Continental origin of the Maha Sarakham evaporites, northeastern Thailand. *J. Southeast Asian Earth Sci.* **8**, 193–207.

Wallmann, K., 2001. Controls on the Cretaceous and Cenozoic evolution of seawater composition, atmospheric CO_2 and climate. *Geochim. Cosmochim. Acta* **65**, 3005–3025.

Ward, W.B., Cox, A., Kwong, M.H., Meyers, W.J., Banner, J.L. 1993. Upper Devonian seawater samples encased in calcite cements: single-phase fluid-inclusion salinities and cement compositions, Devonian reef complexes, Canning Basin, Western Australia (abstract). American Association of Petroleum Geologists 1993 Annual Meeting Program. pp. 197–198.

Wardlaw, N.C., 1972a. Unusual marine evaporites with salts of calcium and magnesium chloride in Cretaceous basins of Sergipe, Brazil. *Econ. Geol.* **67**, 156–168.

Wardlaw, N.C., 1972b. Syn-sedimentary folds and associated structures in Cretaceous salt deposits of Sergipe, Brazil. *J. Sediment. Petrol.* **42**, 572–577.

Wardlaw, N.C., Nicholls, G.D. 1972. Cretaceous evaporites of Brazil and west Africa and their bearing on the theory of continent separation. In: *24th International Geological Congress*, sec. 6. pp. 43–55.

Wheat, C.G., Mottl, M.J., 2000. Composition of pore and spring waters from Baby Bare: global implications of geochemical fluxes from a ridge flank hydrothermal system. *Geochim. Cosmochim. Acta* **64**, 629–642.

Wilkinson, B.H., Owen, R.M., Carroll, A.R., 1985. Submarine hydrothermal weathering, global eustasy, and carbonate polymorphism in Phanerozoic marine oolites. *J. Sediment. Petrol.* **55**, 171–183.